Taylor & Francis
Taylor & Francis Group

Check for updates

In silico identification of widely used and well-tolerated drugs as potential SARS-CoV-2 3C-like protease and viral RNA-dependent RNA polymerase inhibitors for direct use in clinical trials

Seref Gul[a], Onur Ozcan[b], Sinan Asar[c], Alper Okyar[d], Ibrahim Barış[b] and Ibrahim Halil Kavakli[a,b]

[a]Department of Chemical and Biological Engineering, Koc University, Istanbul, Turkey; [b]Department of Molecular Biology and Genetics, Koc University, Istanbul, Turkey; [c]Department of Anesthesiology and Reanimation, Bakırköy Dr. Sadi Konuk Training and Research Hospital, University of Health Sciences, Istanbul, Turkey; [d]Department of Pharmacology, Istanbul University Faculty of Pharmacy, Istanbul, Turkey

Communicated by Ramaswamy H. Sarma

ABSTRACT

Despite strict measures taken by many countries, severe acute respiratory syndrome coronavirus 2 (SARS-CoV-2) continues to be an issue of global concern. Currently, there are no clinically proven pharmacotherapies for coronavirus disease 2019, despite promising initial results obtained from drugs such as azithromycin and hydroxychloroquine. Therefore, the repurposing of clinically approved drugs for use against SARS-CoV-2 has become a viable strategy. Here, we searched for drugs that target SARS-CoV-2 3C-like protease (3CL^{pro}) and viral RNA-dependent RNA polymerase (RdRp) by in silico screening of the U.S. Food and Drug Administration approved drug library. Well-tolerated and widely used drugs were selected for molecular dynamics (MD) simulations to evaluate drug-protein interactions and their persistence under physiological conditions. Tetracycline, dihydroergotamine, ergotamine, dutasteride, nelfinavir, and paliperidone formed stable interactions with 3CL^{pro} based on MD simulation results. Similar analysis with RdRp showed that eltrombopag, tipranavir, ergotamine, and conivaptan bound to the enzyme with high binding free energies. Docking results suggest that ergotamine, dihydroergotamine, bromocriptine, dutasteride, conivaptan, paliperidone, and tipranavir can bind to both enzymes with high affinity. As these drugs are well tolerated, cost-effective, and widely used, our study suggests that they could potentially to be used in clinical trials for the treatment of SARS-CoV-2-infected patients.

1. Introduction

Coronaviruses (CoVs), a large family of single-stranded RNA viruses, can be transmitted from animals to humans, potentially resulting in serious upper respiratory tract disease (Su et al., 2016). The first CoV-related outbreak, caused by the severe acute respiratory syndrome coronavirus (SARS-CoV), was observed in China between 2002 and 2003 (Drosten et al., 2003; Ksiazek et al., 2003). A decade later, Middle East Respiratory Syndrome coronavirus (MERS-CoV) was isolated in patients displaying symptoms of pneumonia in Middle Eastern countries (Zaki et al., 2012). More recently, a novel coronavirus SARS-CoV-2, the causative agent of coronavirus disease 2019 (COVID-19), has emerged in Wuhan, China, becoming a global health issue (WHO, 2020).

Sequence analysis of the full-length genome of SARS-CoV-2 shows 96% identity to bat coronavirus (Wu, Zhao, et al., 2020; Zhou et al., 2020). SARS-CoV-2 contains a linear (+)sense ssRNA genome that encodes proteins commonly produced coronaviruses (Wu, Liu, et al., 2020; Wu, Zhao, et al., 2020) and analyses of its genome organization suggests conserved RNA synthesis machinery and viral life cycle.

All coronaviruses consist of genes encoding the following components: replicase (Rep 1a and 1b), spike (S), envelope (E), membrane (M), and nucleoprotein (N) (Graham et al., 2008; Habibzadeh & Stoneman, 2020; Ziebuhr, 2005). They also possess genes encoding non-structural proteins (nsps) placed between these genes (Gorbalenya et al., 2006). The replication of coronavirus in the cell is initiated by the translation of two overlapping open reading frames (ORF1a and ORF1b) (Scandella et al., 2006; St John et al., 2015; Su et al., 2016; Ziebuhr, 2005) to produce pp1a and pp1ab, generated by a (−)1 ribosomal frameshift mechanism (Firth & Brierley, 2012). These polyproteins are then proteolytically processed by two essential viral cysteine proteases, papain-like protease (PL^{pro}, or nsp3) and 3C-like protease (3CL^{pro}, also known as the main protease, M^{pro}, or nsp5) (Thiel et al., 2003; Ziebuhr, 2004). Cleavage of pp1a and pp1ab by these proteases results in the production of 16 nsps, with PL^{pro} and 3CL^{pro} responsible for cleavage at three and 11 sites, respectively (Prajapat et al., 2020). Nsp12 is the first protein encoded by ORF1b and has viral RNA-dependent RNA polymerase (RdRp) activity (Xu et al., 2003), requiring nsp7 and nsp8 co-factors for maximal activity (Kirchdoerfer & Ward, 2019). The nsp12-

nsp7-nsp8 complex is responsible for transcribing both positive and negative RNA strands (Thiel et al., 2003).

The viral life cycle has multiple stages, including entry, replication of genetic material, protein translation, assembly, and release. Strategies for drug development, which includes computer-aided drug design, aim at targeting viral proteins and host receptors in order to interfere with different stages of the coronavirus life cycle (Boopathi et al., 2020; Das et al., 2020; Khan et al., 2020; Li et al., 2020; Sarma et al., 2020). Given the crucial role of RdRp and 3CL[pro] in the virus life cycle, these proteins are seen as promising drug targets. Similar approaches have yielded promising drugs against viruses such as human immunodeficiency virus (HIV) and hepatitis C virus (HCV) (De Clercq, 2007). Here, we performed in silico drug repurposing to find candidate drugs that may inhibit the enzymatic activity of 3CL[pro] and RdRp by using the U.S. Food and Drug Administration (FDA) approved drug library. Our study revealed 360 and 850 drugs with high affinity (< -7.5 kcal/mol) to 3CL[pro] and RdRp, respectively. After the identification of the drugs which may have potential to bind both viral enzymes, we performed detailed literature analysis to determine well-tolerated drugs that have demonstrated in vitro antiviral activity against other viruses. We found several drugs that may be directly used in clinical trials: antibiotic tetracycline and its derivatives, migraine drugs ergotamine and dihydroergotamine, vasopressin receptor antagonists conivaptan and tolvaptan, antiandrogen dutasteride, and trombopoetin receptor agonist eltrombopag. Our results suggest that these drugs may be used alone or in combination as adjuvants with current protocols for the treatment of SARS-CoV-2.

2. Materials and methods

2.1. Protein and ligand preparation for docking simulations

We initially performed pairwise multiple sequence alignment to determine the degree of conservation among SARS-CoV-2 and other coronavirus family members for 3CL[pro] and RdRp using EMBL-EBI server (Madeira et al., 2019) and JalView (2.11.0). SARS-CoV RdRp (PDB ID: 6NUR) and 3CL[pro] (PDB ID: 6Y84) (Owen et al., 2020) structures were retrieved from The Protein Data Bank (www.rcsb.org) and used in docking studies. Proteins were prepared for docking simulations via UCSF Chimera, Dock Prep module as described in (Tardu et al., 2016). Excess water molecules and, in case of presence of alternate locations for residues, the ones with the lower occupancies were removed from structures. Any missing side chains were completed by using the Dunbrack 2010 rotamer library. Polar hydrogens were added. Next, non-polar hydrogens were merged with atoms that they are bound. Finally, Gasteiger charges were introduced to structures with Auto Dock Tools (ADT) suite. Structures of drugs were obtained from Zinc15 database catalogue of FDA-approved drugs that are imported from the compounds within the U.S. Environmental Protection Agency's (EPA) Distributed Structure-Searchable Toxicity (DSSTox) database. The 3948 drugs and inhibitors of HKU4-CoV 3CL[pro] were prepared for

docking by using ADT suite. Active site of 3CL[pro] containing the catalytic dyad (Cys[145] and His[41] in SARS-CoV-2) was used as grid center for docking simulations of the protease. The binding site of nsp8 protein was identified as the grid center for RdRp (centering Thr[324] and Val[330] residues). Grid box sizes for the 3CL[pro] and RdRp are determined as 4050 Å^3 and 9600Å^3, respectively. All docking studies were performed via AutoDock Vina (version 1.1.2) (http://vina.scripps.edu/) (Trott & Olson, 2010).

2.2. Molecular dynamics simulations and calculation of binding free energy

Protein structures were solvated in a rectangular box with size of 1.04×10^6 Å^3 and 3.97×10^5 Å^3 using TIP3P water molecules for RdRp and 3CL[pro], respectively. Systems were neutralized with sodium and chloride ions and then additional 150 mM Na$^+$ Cl$^-$ ions were added to system to simulate physiological conditions (Humphrey et al., 1996). Energy minimization was performed for 20,000 steps by conjugate gradient method. Systems was gradually heated and equilibrated in NPT ensemble for 1.4 ns. Throughout equilibration, constrains on the proteins were gradually removed starting from 2 kcal/mol/Å^2. At each stage constrains were reduced by 0.5 kcal/mol/Å^2 and system were equilibrated for 0.4 ns. After equilibration, a production run of 20 ns for each complex was performed. Time step was set to 2fs. van der Waals (12 Å cut-off) and long-range electrostatic interactions (via particle-mesh Ewald) were included to calculate the force acting on the system. Production runs were performed at 310 K and under 1 atm pressure using a Langevin thermostat and a Langevin barostat for 20 ns, respectively. All simulations were performed by using NAMD (Phillips et al., 2005) software and CHARMM36m forcefield (Huang et al., 2017). The numerical calculations reported in this paper were partially performed at TUBITAK ULAKBIM, High Performance and Grid Computing Center (TRUBA resources). All analysis of MD simulations were performed using VMD, and protein representations were prepared by using Pymol (DeLano, 2009). Parameters of drugs for molecular simulations were generated through CHARMM-GUI (Jo et al., 2008; Kim et al., 2017). Structural analysis of proteins and protein-drug interactions were reported by i) calculating Root Mean Square Deviation (RMSD) of proteins, ii) analyzing the contact frequencies between residues and drugs, iii) calculating distances between centroid (geometric center) of drugs and Cα atoms of target residues, and iv) calculating binding free energies of drugs to target proteins as functions of time. RMSD of simulations and contact frequencies were calculated by using RMSD trajectory tool and timeline functions in VMD, respectively.

Binding free energy (BFE) of drugs (8 for 3CL[pro] and 4 for RdRp) were calculated by molecular mechanics generalized born surface area (MM/GBSA) method. MMPBSA.py script of AmberTools18 was used for MM/GBSA calculations (Case et al., 2018). For each calculation, 1000 frames obtained from 20 ns simulations were used. BFE between drug and protein is calculated based on Equation 1:

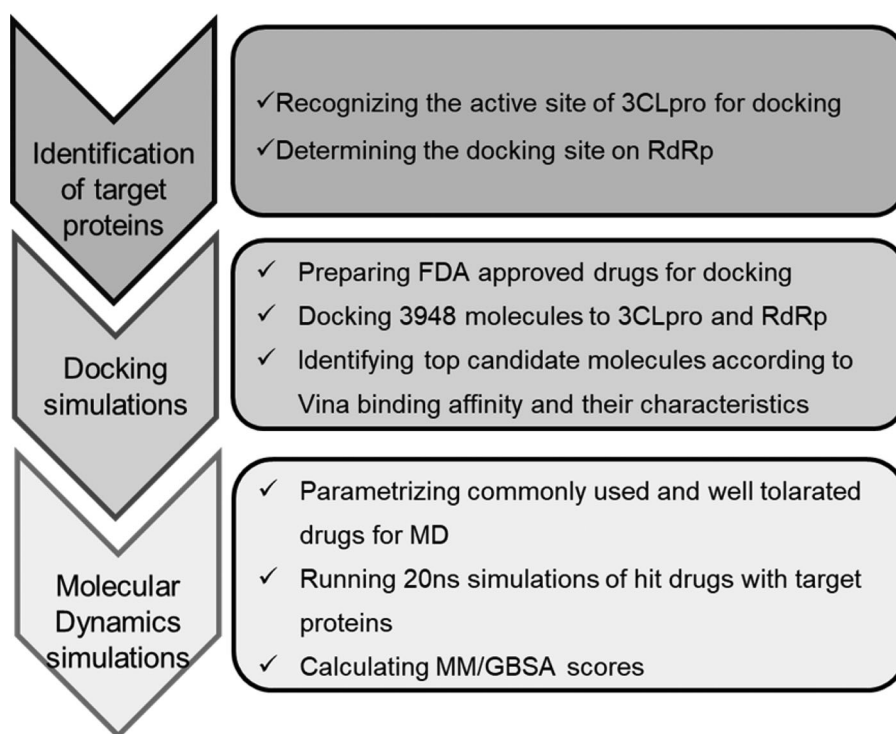$$\Delta G_{binding} = G_{complex} - G_{receptor} - G_{ligand} \qquad (1)$$

Figure 1. Outline of the study.

where $G_{complex}$ represents the energy of protein-drug complex, $G_{receptor}$ and G_{ligand} represent the energies of protein and drug in their unbound states, respectively. Each energy term consists of mechanical energy term (E_{MM}), solvation energy term (G_{solv}), and entropic term (TS) (Equation 2). In detail, E_{MM} includes electrostatic, van der Waals and bounded energy terms; G_{solv} includes polar and nonpolar solvation terms, and TS includes vibrational, rotational and translational energy terms.

$$G = (E_{electrostatic} + E_{vdw} + E_{bonded}) + (G_{polar} + G_{nonpolar}) - (TS_{vibration} + TS_{rotation} + TS_{translation})$$

$$(2)$$

3. Results and discussion

3.1. Selection of target proteins

Various strategies can be used to develop antiviral drugs, such as blocking viral binding to human cell receptors and inhibiting viral replication and self-assembly (Boopathi et al., 2020; Islam et al., 2020; Khan et al., 2020; Li et al., 2020; Sk et al., 2020; Wu, Liu, et al., 2020). Essential SARS-CoV-2 proteins 3CL^{pro} and RdRp (nsp12) are prime targets due to their function in viral polyprotein processing and genome replication, respectively (Gorbalenya et al., 2006; Wu, Zhao, et al., 2020). The FDA-approved drug library was used to screen for the identification of molecules with high affinity to the active site of 3CL^{pro} and nsp8 binding site of RdRp (Figure 1).

Multiple sequence alignments of 3CL^{pro} amino acid sequences from SARS-CoV, MERS-CoV, HKU4, and SARS-CoV-2 revealed the conservation of a catalytic dyad (Cys^{148} and His^{41}) (Figure 2(A)). The crystal structure of SARS-CoV-2 3CL^{pro} has recently been released (PDB ID: 6y84; (Owen

et al., 2020). Comparison of this structure with SARS-CoV (Anand et al., 2003) and MERS-CoV 3CL^{pro} (Tomar et al., 2015) showed high structural identity (Figure 2(B)). Experimental verification of the active site was confirmed by developing inhibitory molecules against HKU4 3CL^{pro} (St John et al., 2015). Based on this information, we targeted the catalytic dyad pocket of 3CL^{pro} for in silico screening (Figure 2(C)).

RdRp requires interaction with nsp7 and nsp8 for maximal activity. The crystal structure of the SARS-CoV RdRp-nsp7-nsp8 complex has been solved (Kirchdoerfer & Ward, 2019). This enabled us to identify the critical region of RdRp that interacts with co-factor nsp8 (Figure 3(A)). Alignment of RdRp amino acid sequences from SARS-CoV and SARS-CoV-2 exhibited 95% identity, while RdRp residues that interact with nsp8 are 100% conserved (shown in rectangular boxes in Figure 3(B)). Thus, we targeted the nsp8 binding site of RdRp for in silico screening with a goal to find molecules that inhibit the interaction between RdRp and nsp8 and, in turn, may interfere with the replisome activity.

3.2. Strategy of identification of candidate drugs

FDA approved drugs were retrieved from the ZINC database (http://zinc15.docking.org/catalogs/fda) and prepared for docking simulations (Irwin & Shoichet, 2005). Virtual screening was performed as described previously (Armutlu et al., 2009; Çakir et al., 2012; Doruk et al., 2020). AutoDock Vina was used to predict the optimal conformations of the receptor-ligand complex. Binding affinity energies were calculated by assuming a rigid receptor (protein) and a flexible ligand. To determine a cut-off value that could be used for the identification of drugs with high
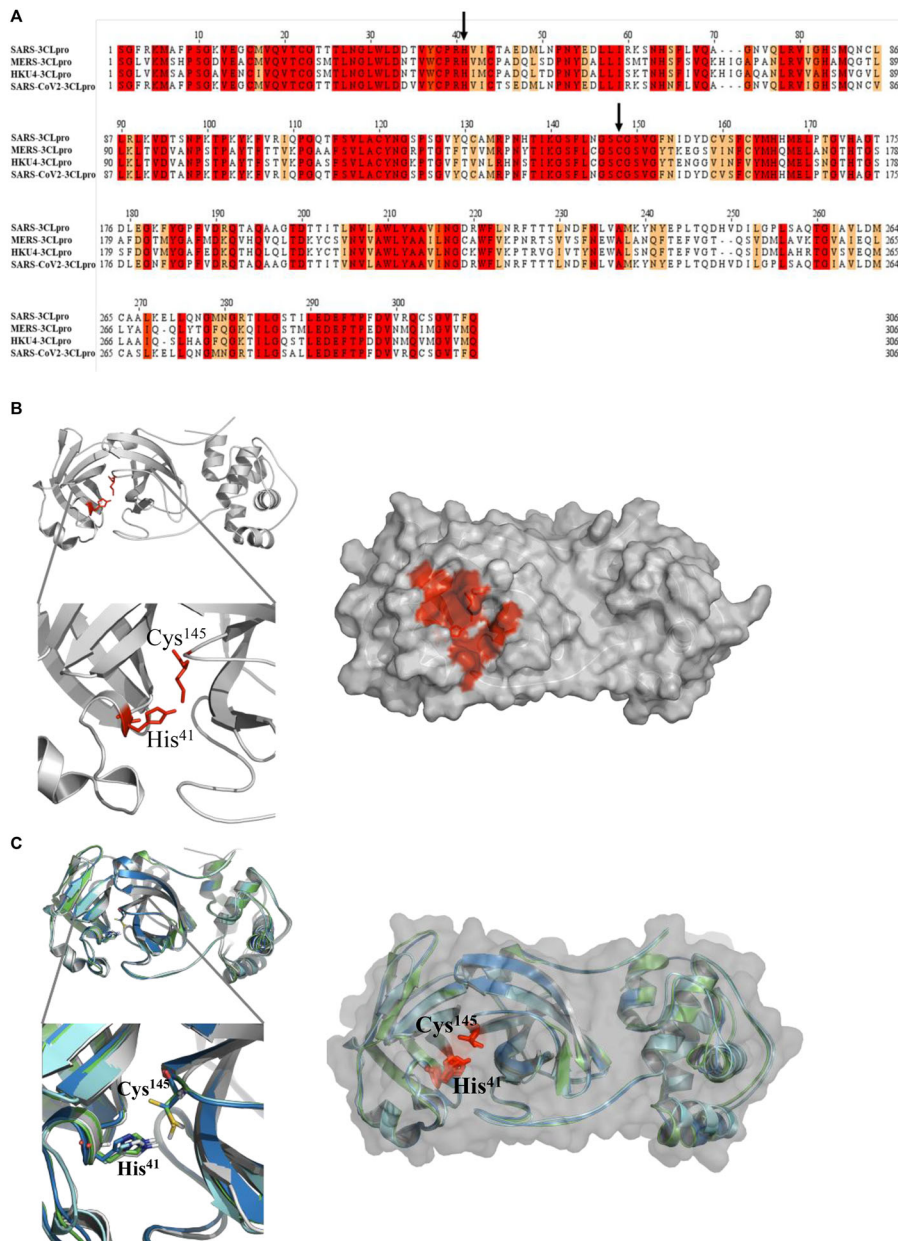
Figure 2. The structure of 3 chymotrypsin like protease (3CL[pro]) **A)** Sequence alignment of 3CL[pro] from SARS-CoV, MERS, HKU and SARS-CoV2 viruses. Conserved residues are highlighted in red. Arrows show the conserved residues (His[41] and Cys[145]) which are critical for the protease activity. **B)** Superimposing the crystal structures of 3CL[Pro] from SARS shown in cyan (PDB ID: 3VB3), MERS shown in green (PDB ID: 4ylu), HKU4 shown in navy (PDB ID: 4yo9) and SARS-CoV-2 shown in white (PDB ID: 6y84) cartoon (left) or surface representations (right). Conserved catalytic residues (His[41] and Cys[145]) are shown in red stick representation. **C)** Catalytic pocket of SARS-CoV-2 of 3CL[pro] is shown in red. Protein is shown in white cartoon (left) or surface (right) (PDB ID: 6y84). Catalytic residues His[41] and Cys[145] are shown with sticks (red) representation.

docking binding energies to 3CL[pro], we calculated binding energies between previously identified HKU4 3CL[pro] inhibitors (4f4, rfm, and 4f5) and 3CL[pro] (St John et al., 2015). As the binding energies of the inhibitors were between −7.5 kcal/mol and −7.0 kcal/mol (Table 1), we set −7.5 kcal/mol as the cut-off value during the selection of drugs from docking simulations. A histogram of Vina binding affinities of all investigated drugs is shown in Figure S1A. We eliminated the possibility of transient interactions between targets and molecules by performing molecular dynamics (MD) simulation for 20 ns. Root-mean-square deviation (RMSD) calculation of Cα atoms for each protein-drug simulation indicated when MD simulations had reached

equilibrium. After initial increases in RMSD values during the first 2 ns of simulations, each equilibrated at approximately 1.5–3 Å (Figure S2). The stability of drug-protein interactions was also verified by visual inspection of MD trajectories. Critical amino acid residues of the target proteins that interact with bound drugs were then identified. Additionally, the distance between the geometric center of individual drugs and interacting amino acid residues were measured. Finally, the binding free energy (BFE) and amino acids that contribute to the BFE of target proteins were calculated from trajectories with the molecular mechanics energies combined with the generalized Born and surface area continuum solvation (MM-GBSA) method.
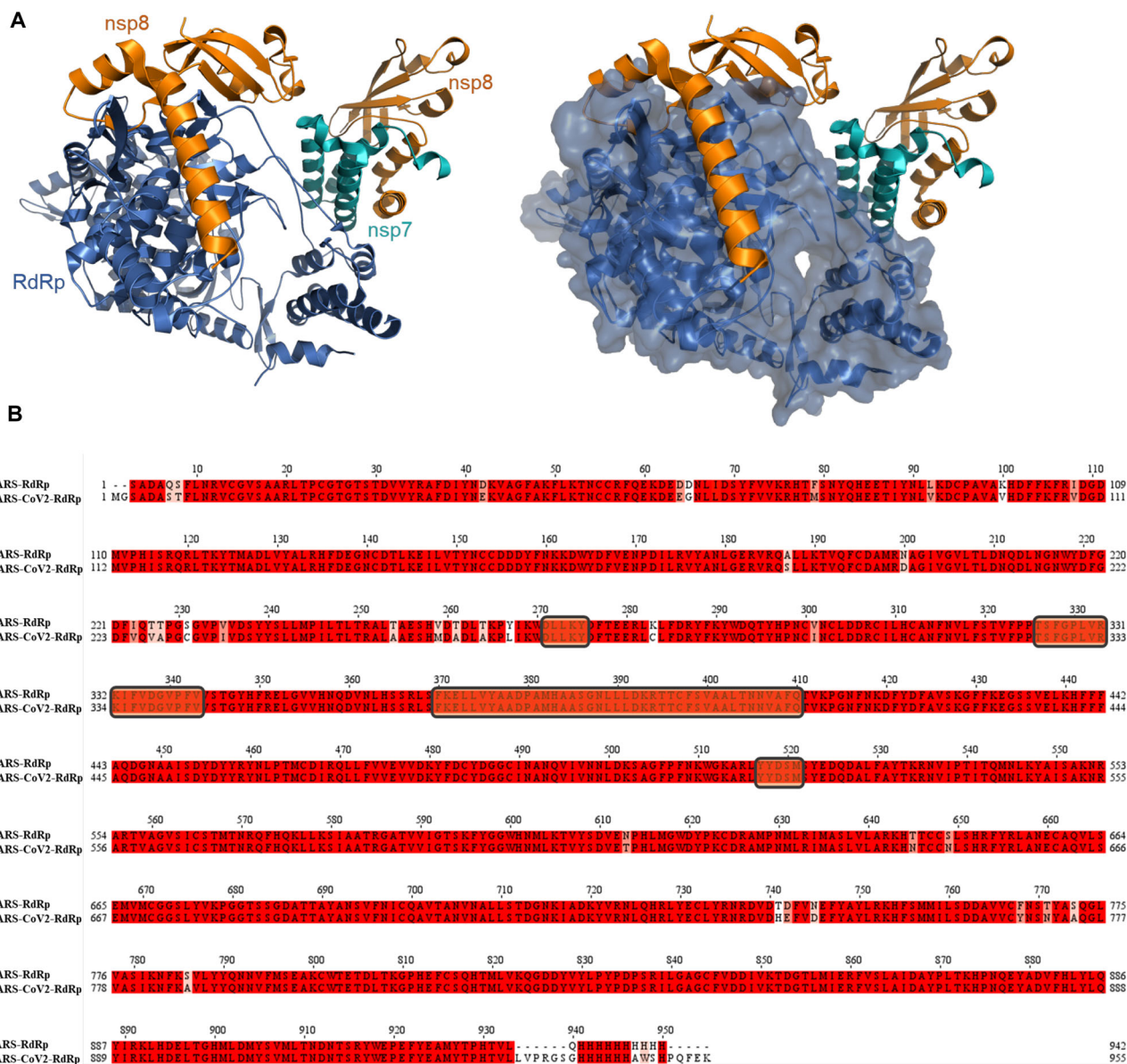
Figure 3. The structure of RNA-dependent RNA polymerase (RdRp) **A)** RdRp is shown in blue cartoon (left) or surface representations (right), binding partners nsp8 are nsp7 are shown in orange and cyan cartoon, respectively (PDB ID:6nur). **B)** Sequence. alignment of RdRp from SARS and SARS-CoV2. Conserved residues are highlighted in red. Residues interacting with nsp8 are indicated with rectangle boxes.
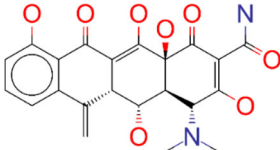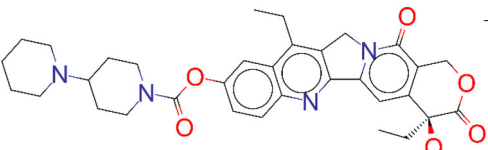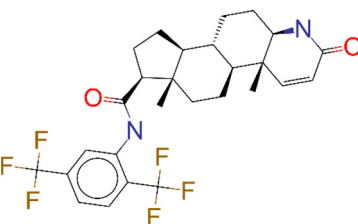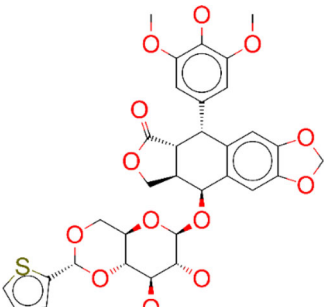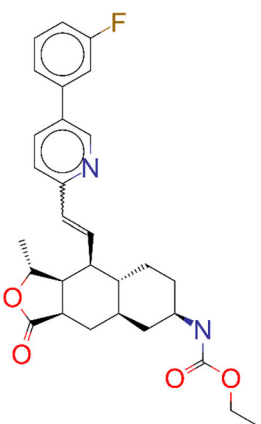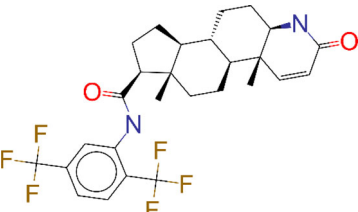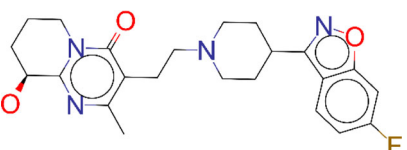
3.3. Docking and MD simulations of selected drugs against SARS-CoV-2 3CL^pro

Docking results of 3CL^pro revealed 360 molecules with docking binding energies less than −7.5 kcal/mol (top 100 molecules are listed in Table S1). The top 15 molecules, with binding energies < −8.6 kcal/mol, are shown in Table 1. A literature survey of the top hits revealed that these drugs have antiviral, antibacterial, anticancer, and analgesic effects. The following drugs were determined as widely used and well tolerated: tetracycline and its derivatives, dutasteride, ergotamine, dihydroergotamine, bromocriptine, nelfinavir, and paliperidone.

In silico analyses revealed that tetracycline and its derivatives exhibit high affinity to 3CL^pro. Docking binding energies of tetracycline, metacycline, doxycycline, oxytetracycline, rolitetracycline, chlortetracycline, and tigecycline were −8.1, −9.1, −8.2, −8.5, −8.2, −8.2, and −6.9 kcal/mol, respectively.

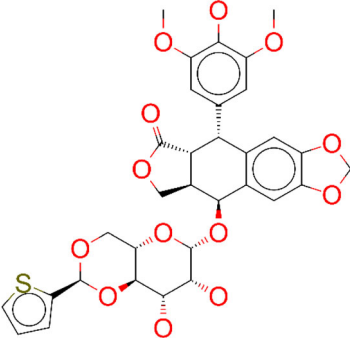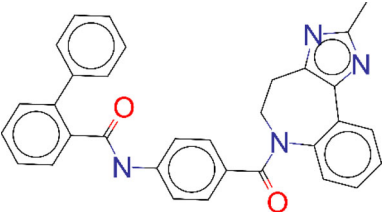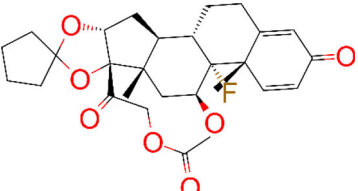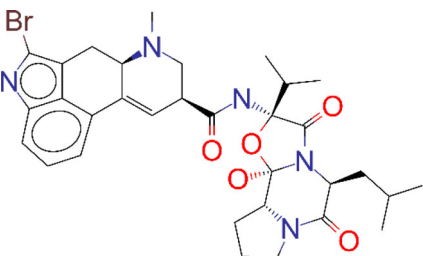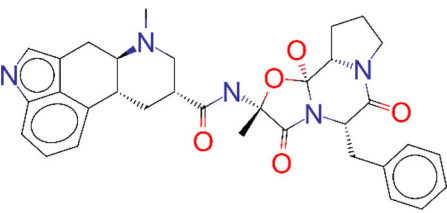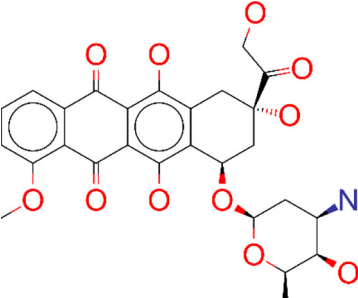In our docking model, tetracycline occupies the catalytic site of 3CL^pro and interacts with catalytically active His^{41} and Cys^{145} residues (Figure 4(A)). In addition, tetracycline interacts with Ser^{46}, Asn^{142}, and Glu^{166} residues, forming hydrogen bonds with Ser^{46} and Glu^{166} (Table 2). We assessed the persistency of interactions between tetracycline and 3CL^pro under physiological conditions by analyzing MD trajectories. We observed that hydrogen bond interactions between tetracycline and Ser^{46}/Glu^{166} were maintained and additional interactions were formed with Met^{49} and Gln^{189} during the simulation (Figure 4(A)). Measuring the distance between critical residues (His^{41}, Met^{49}, and Glu^{189}) and the geometric center of tetracycline further confirmed that the drug kept its initial docking position (Figure 5(A)). We then determined the BFE between tetracycline and 3CL^pro from MD simulations using the MM/GBSA method. The BFE of tetracycline was calculated as −14.6 kcal/mol, which is comparable to the

Table 1. List of top 15 drugs having the best binding affinity to 3CL^{pro} and 3CL^{pro} inhibitors from MERS-CoV.

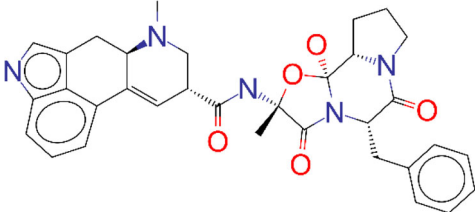| ZINC ID and/or Drug Name	2D Structure	Vina Binding Affinity (kcal/mol)	Pharmacology / Indication
ZINC000084480349 / Metacycline		−9.1	For the treatment of acute bacterial exacerbations of chronic bronchitis
ZINC000001612996 / Irinotecan		−9.1	For the treatment of metastatic colorectal cancer
ZINC000003932831 / Dutasteride		−8.9	Indicated for the treatment of symptomatic benign prostatic hyperplasia (BPH) in men with an enlarged prostate gland
ZINC000004099009 / Teniposide		−8.9	Teniposide is used for the treatment of refractory acute lymphoblastic leukaemia
ZINC000003925861 / Vorapaxar		−8.9	Vorapaxar is indicated for the reduction of thrombotic cardiovascular events in patients with a history of myocardial infarction or peripheral arterial disease
ZINC000003938684 / Etoposide		−8.9	For use in combination with other chemotherapeutic agents in the treatment of refractory testicular tumors
ZINC000004214700 / Paliperidone		−8.8	Used in the treatment of schizophrenia
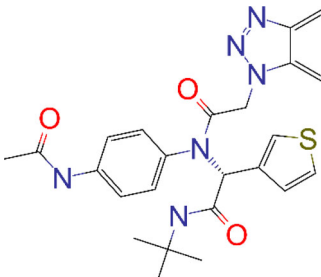
Table 1. Continued.

ZINC ID and/or Drug Name	2D Structure	Vina Binding Affinity (kcal/mol)	Pharmacology / Indication
ZINC000003831508 / Teniposide		−8.8	Teniposide is used for the treatment of refractory acute lymphoblastic leukaemia
ZINC000012503187 / Conivaptan		−8.7	For the treatment of euvolemic or hypervolemic hyponatremia in hospitalized patients
ZINC000003977777 / Amcinonid		−8.7	Shows anti-inflammatory activity
ZINC000059364574 / Bromocriptine		−8.6	For the treatment of galactorrhea due to hyperprolactinemia, prolactin-dependent menstrual disorders and infertility, prolactin-secreting adenomas, prolactin-dependent male hypogonadism
ZINC000003978005 / Dihydroergotamine		−8.6	For the acute treatment of migraine headaches with or without aura and the acute treatment of cluster headache episodes.
ZINC000003830729/ Doxorubicin		−8.6	Doxorubicin is used to produce regression in disseminated neoplastic conditions like acute lymphoblastic leukemia, acute myeloblastic leukemia, Wilms' tumor, neuroblastoma, soft tissue and bone sarcomas, breast carcinoma, ovarian carcinoma etc.

(continued)

BFEs of control molecules 4f4 and 4f5 (−16.71 kcal/mol and −24.96 kcal/mol, respectively) (Figures S3 and S4). Detailed energy decomposition analysis showed that tetracycline had the highest binding affinity to His[41] and Met[49] located in the active site of the protease (Figure 6), which was similar to the control molecules (Figure S5).
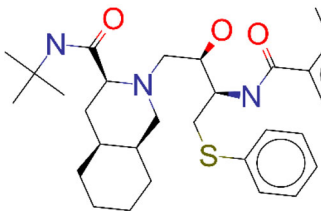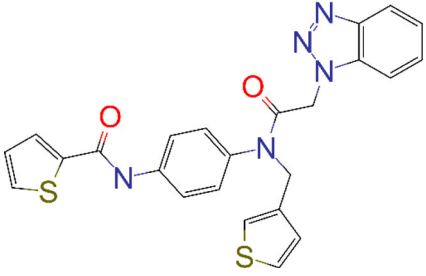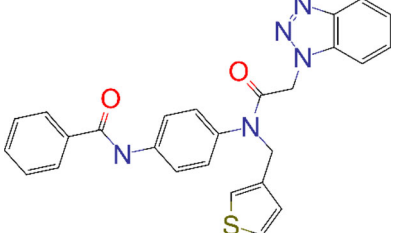
Table 1. Continued.

ZINC ID and/or Drug Name	2D Structure	Vina Binding Affinity (kcal/mol)	Pharmacology / Indication
ZINC000052955754 / Ergotamine		−8.6	For use as therapy to abort or prevent vascular headache
ZINC000003833846/ Nelfinavir		−8.6	Used in combination with other antiviral drugs in the treatment of HIV in both adults and children
4F4		−7.5	Inhibitor of 3CL in MERS
RFM		−7.5	
4F5		−7.0	

Notably, several in vitro screening studies have reported that doxycycline exhibits antiviral activity. Doxycycline is well tolerated, has great distribution to tissues, and has a bioavailability of over 80% when taken orally (Agwuh & MacGowan, 2006; Smilack, 1999). Consistent with our tetracycline results, doxycycline and other derivatives oxytetracycline and tigecycline were shown to exhibit high binding affinity to 3CLpro in a recent in silico study (Wu, Liu, et al., 2020). Doxycycline significantly inhibited viral propagation of vesicular stomatitis virus (VSV), porcine reproductive and respiratory syndrome virus (PRRSV), and replication of dengue viruses (DENV1-4) (Li et al., 2017; Rothan et al., 2014; Wu et al., 2015). These studies suggest that doxycycline may

have a broader activity as an antiviral agent, in addition to its well-defined bacteriostatic activity.

Ergotamine and its derivative dihydroergotamine exhibited high affinity to 3CLpro with docking binding energy of −8.6 kcal/mol. In our docking models, dihydroergotamine bound to 3CLpro in a U-shaped form by means of His[41], Cys[145], Thr[25], Thr[26], Ser[46], and Glu[189] residues (Figure 4(B)), with hydrogen bond formation observed with Thr[25]/Glu[189] (Table 2). MD simulations confirmed that interactions between the molecule and Thr[25]/His[41]/Met[49]/Ser[46] were strong and stable (Figure 4(B)). Additionally, initial distances were maintained within 1–2 Å fluctuations, with a BFE of −16.22 kcal/mol, as calculated by MM/GBSA analysis (Figure
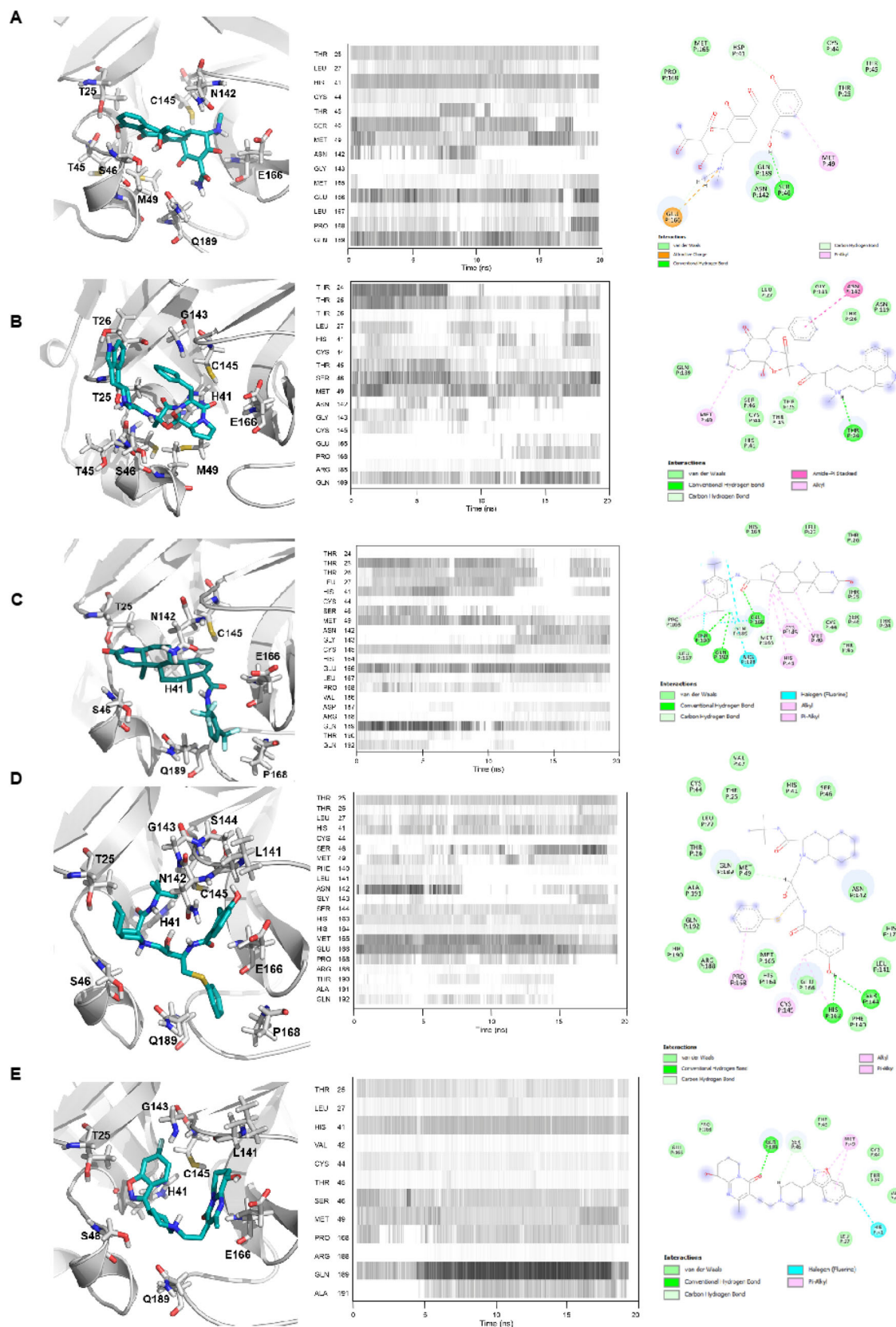
Figure 4. Binding mode of top 4 candidate drugs to SARS-CoV-2 3CL^pro. **A)** tetracycline **B)** dihydroergotamine **C)** dutasteride, **D)** nelfinavir, and **E)** paliperidone. Docking position of each drug is shownat left panels. Proteins are shown in ribbon and drugs are shown with stick representations.20 ns MD simulations were performed and the frequency of interacting amino acid residues are shown in middle panels. Right panel shows the amino acid resides of the SARS-CoV-2 3CL^pro that interacts with drugs after molecular simulations. The following coloring scheme is used in figures: carbons are white, nitrogens are blue, oxygens are red, sulphurs are yellow, however, carbons in ligands are shown in cyan.

Table 2. Interacting residues of selected drugs with 3CL^{Pro}.

Drug	Interacting residues
Tetracycline	Thr26, His41, Cys45, Ser46, Met49, Asn142, Met165, Glu166, Gln189
Dihydroergotamine	Thr25, Thr26, His41, Thr45, Ser46, Met49, Gly143, Cys145
Dutasteride	Thr25, His41, Ser46, Asn142, Cys145, Glu166, Pro168, Gln189
Nelfinavir	Thr25, His41, Ser46, Leu141, Asn142, Gly143, Ser144, Cys145, Glu166, Pro168, Gln189
Paliperidone	Thr25, His41, Ser46, Leu141, Gly143, Cys145, Glu166, Gln189
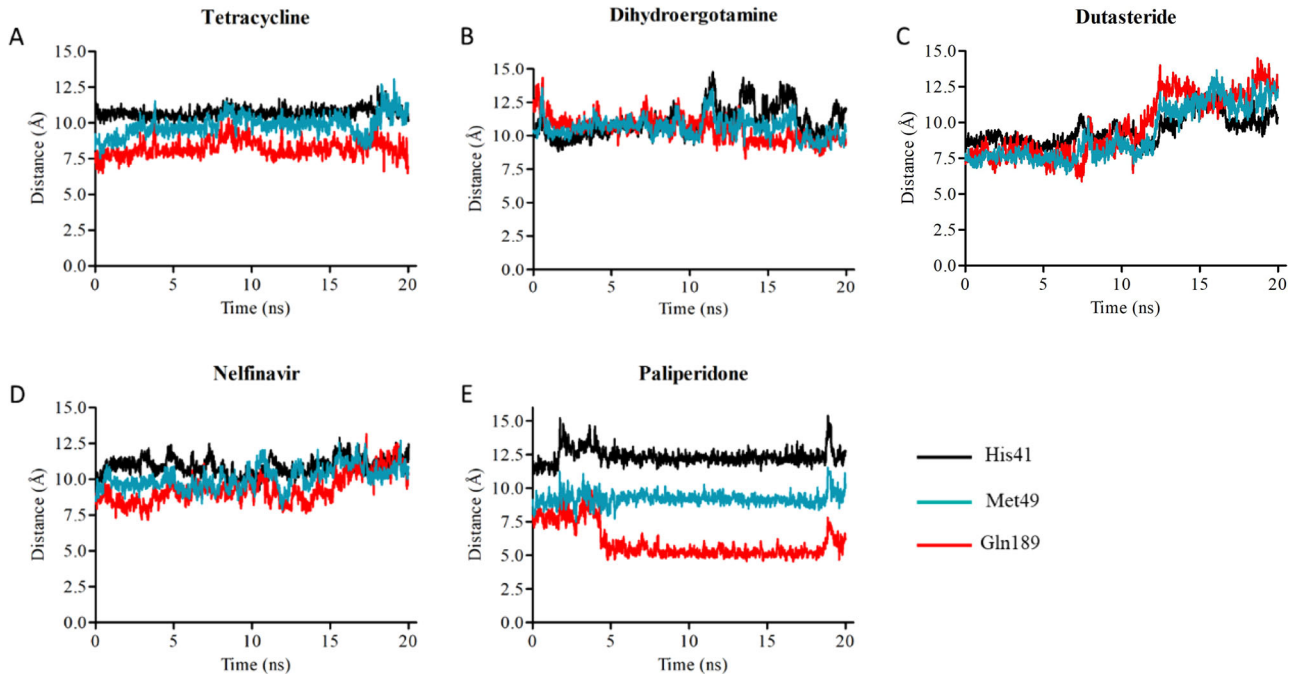
Figure 5. Distance between geometric center of drugs A) tetracycline, B) dihydroergotamine, C) dutasteride, D) nelfinavir, E) paliperidone and Cα atoms of critical residues (His^{41}, Gln^{189}, and Met^{49}) on 3CL^{pro}.
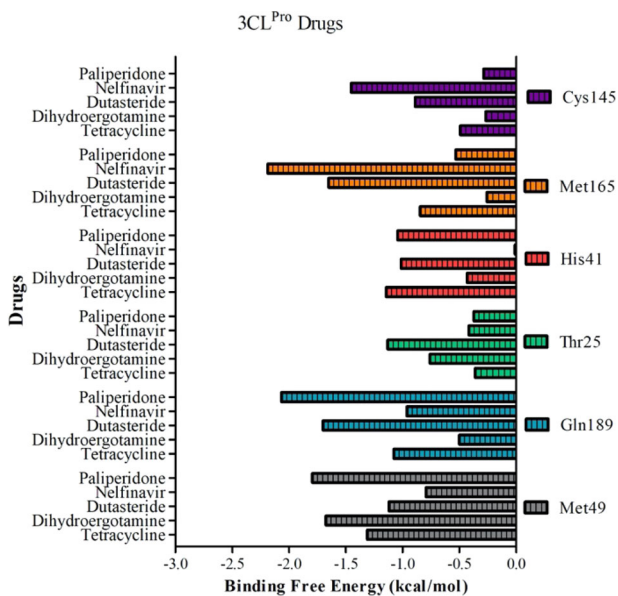
Figure 6. Contribution of each residue to binding free energy in drug-3CL^{pro} simulations.

5(B)). Energy decomposition analyses further showed that Met^{49}/Glu^{189}/Thr^{25} had the highest contributions to the BFE (Figure 6). Ergotamine is an α-1 selective adrenergic agonist and is commonly used in the treatment of migraine disorders (Silberstein, 1997). Double-blind, randomized, placebo-controlled, parallel-group, multi-center studies indicate that ergotamine and dihydroergotamine are well tolerated and adverse events are generally mild or moderate and transient (Christie et al., 2003; Diener et al., 2002). However, combining ergotamine with protease inhibitors, such as nelfinavir and indinavir, is not advised due to potential cross-interaction through CYP3A4 (Mortier et al., 2001; Rosenthal et al., 1999). Bromocriptine is another semisynthetic ergot alkaloid derivative and functions as a dopamine receptor agonist and serotonin modulator (Kvernmo et al., 2006). Clinically, bromocriptine is used to treat hyperprolactinemia and Parkinson's disease (Kvernmo et al., 2006; Via et al., 2010). Here, bromocriptine showed high binding affinity against both RdRp and 3CL^{pro}, with −9.2 kcal/mol and −8.6 kcal/mol docking binding energies, respectively. Several in vitro and in vivo studies have shown that bromocriptine inhibits Zika virus NS2B-NS3 protease activity and interferes with dengue virus post-translation and/or RNA synthesis by interacting with the NS3 helicase (Chan et al., 2017; Kato et al., 2016; Yuan et al., 2017). However, a recent study tested bromocriptine in the Vero E6 cellular infection model and found no suppression of SARS-CoV-2 viral replication, even at doses of 100 μM (Lo et al., 2020).

Dutasteride is an oral synthetic 4-azasteroid and displays antiandrogenic activity by blocking type I and II 5α-reductase, enzymes responsible for converting testosterone into dihydrotestosterone (DHT), a primary hormonal mediator

Table 3. MM/GBSA BFE of protease inhibitors and promising drugs to interfere with SARS-CoV-2 3CL^{pro} and RdRp activities.

3Clpro		RdRp	
Drug Name	MM/ GBSA BFE (kcal/mol)	Drug Name	MM/ GBSA BFE (kcal/mol)
Tetracycline	−15.19 ± 2.76	Ergotamine	−24.65 ± 3.93
Dihydroergotamine	−16.22 ± 5.41	Eltrombopag	−35.33 ± 3.48
Dutasteride	−20.47 ± 6.29	Conivaptan	−23.83 ± 5.43
Nelfinavir	−26.28 ± 4.48	Tipranavir	−26.08 ± 3.86
Paliperidone	−18.23 ± 4.17		
4F4	−16.71 ± 4.66		
4F5	−24.96 ± 3.63		

that plays a role in the development and enlargement of the prostate gland (Andriole & Kirby, 2003; Clark et al., 2004). Dutasteride was approved by the FDA in 2001 for the treatment of symptomatic benign prostatic hyperplasia (BPH). Large open-label extension studies revealed that dutasteride is well tolerated and drug-related adverse events are reported in less than 2% of patients (Marberger, 2006; Roehrborn et al., 2002; Thomson, 2005). Docking analyses revealed that dutasteride has a high docking binding energy of −8.9 kcal/mol against 3CL^{pro} (Figure 4(C)).

The BFE of nelfinavir, an HIV-1 protease inhibitor drug, to the target was calculated as −8.6 kcal/mol (Figure 4(D)). Interestingly, nelfinavir strongly inhibits replication of SARS-CoV (Yamamoto et al., 2004). Furthermore, a recent study showed that nelfinavir mesylate drastically inhibits cell-to-cell fusion in transiently transfected Vero cells with plasmids expressing SARS-CoV-2 spike protein (Musarrat et al., 2020).

Binding poses of dutasteride and nelfinavir in docking simulations displayed similarities. Both interact with the aforementioned tetracycline and dihydroergotamine binding polar residues via the 1,4-bis(trifluoromethyl) benzene and benzyl moieties of dutasteride and nelfinavir, respectively. While dutasteride forms hydrogen bond interactions with Thr^{25} and Glu^{166}, nelfinavir can only interact with Glu^{166} of 3CL^{pro} (Figure 4(C, D)) (Table 2). Contact analysis from MD simulations showed that dutasteride forms stable interactions with Thr^{25}, Met^{49} and Glu^{189}, and His^{41} and nelfinavir interacts with Met^{165} and Glu^{189} (Figure 4(C, D)). Despite deviations of dutasteride from its initial docking pose, its localization in the active site was verified by visual inspection (Figure 5(C)). Analyzing the distance between critical amino acid residues and nelfinavir indicated that its initial docking orientation was maintained throughout the MD simulation (Figure 5(D)). Met^{49}, Cys^{145}, Met^{165}, and Glu^{189} are common residues that interact most favorably with dutasteride and nelfinavir, resulting in BFEs of −20.47 and −26.28 kcal/mol, respectively (Figure 6) (Table 3). These observations suggest that both drugs interact strongly with catalytically active Cys^{145} and other residues in the active site of 3CL^{pro}, and may inhibit protease activity.

Paliperidone is an oral antipsychotic for the treatment of schizophrenia (Janicak & Winans, 2007). Three six-week trials in patients with acute schizophrenia reported that an extended release form of paliperidone is effective and well tolerated, compared with placebo (Davidson et al., 2006; Marder et al., 2007), undergoing limited hepatic metabolism thereby minimizing the risk of hepatic drug-drug interactions (Janicak & Winans, 2007). Paliperidone showed high binding
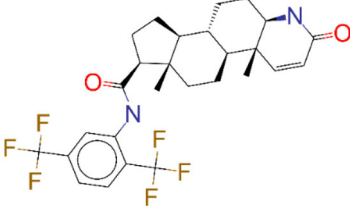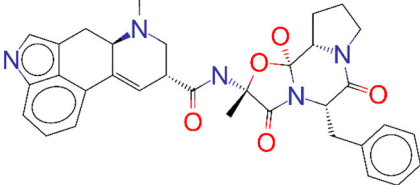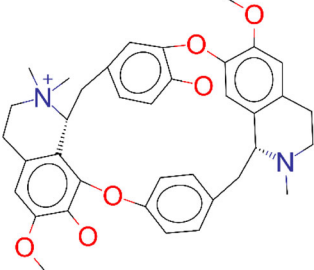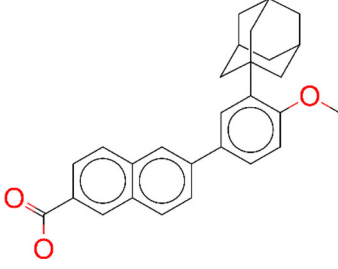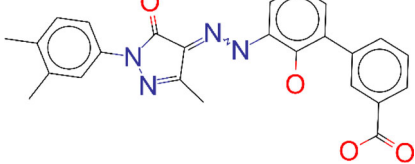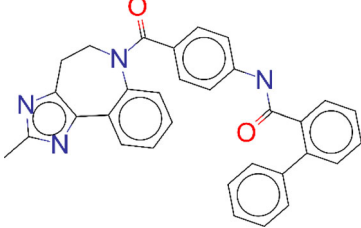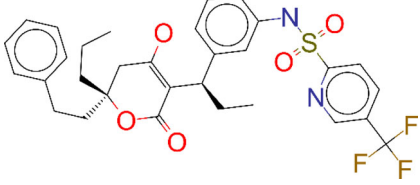
affinity against both 3CL^{pro} and RdRp, with docking binding energies of −8.8 kcal/mol and −8.6 kcal/mol, respectively. Similar to dihydroergotamine, paliperidone binds to 3CL^{pro} in a U-shaped conformation and interacts with polar residues Thr^{25}, His^{41}, Met^{49}, and Gln^{189} (Figure 4(E)). Consistent with interactions observed in the docking conformation, paliperidone interacted with these polar residues through almost the entirety of the MD simulation (Figure 4(E)). Distance analysis between critical residues and paliperidone suggested that the molecule adjusted its position as the simulation progressed. While paliperidone kept its initial distance to His^{41} and Met^{49}, it got closer to Gln^{189} during the simulation (Figure 5(E)). Paliperidone exhibited high affinity with a BFE of −18.23 kcal/mol as assessed by MM/GBSA analysis. Additional energy decomposition analysis confirmed that Glu^{189}, Met^{49}, and His^{41} contributed favorably to the binding energy (Figure 6).

We validated our results by docking other antiviral drugs lopinavir and ritonavir, which have docking binding energies of −7.7 kcal/mol and −6.8 kcal/mol to 3CL^{pro}, respectively. Lopinavir and ritonavir are antiretroviral protease inhibitors used in combination with other antiretrovirals in the treatment of HIV-1 infections. In vitro studies have shown that a combination of lopinavir and ritonavir can inhibit the replication of MERS-CoV and SARS-CoV to exert antiviral effects (Dyall et al., 2017). There are also several reports on the use of Kaletra (lopinavir/ritonavir) for the treatment of COVID-19 infections (He et al., 2020; Lim et al., 2020).

MD simulations of selected drugs showed that interactions between these drugs and 3CL^{pro} are not transient but stable. Furthermore, comparable or better BFE values of selected drugs with respect to known inhibitors indicate that these drugs have high potential to interfere with 3CL^{pro} activity. We also determined critical residues responsible for the high binding affinity of drugs to the protease, which may help to develop novel inhibitor molecules through rational drug design and quantitative structure-activity relationship (QSAR) studies.
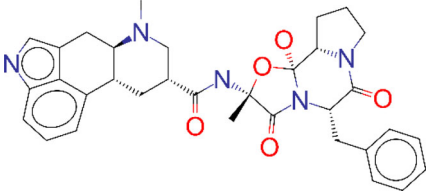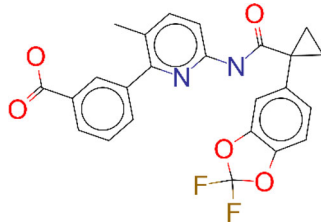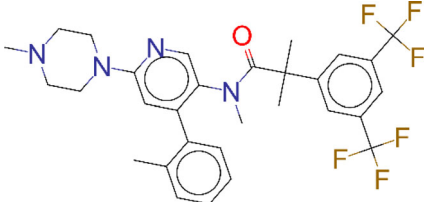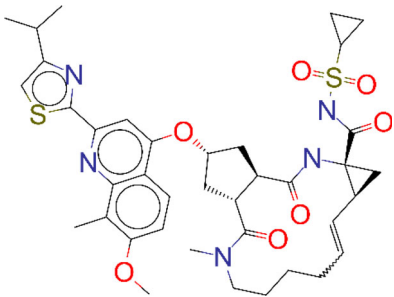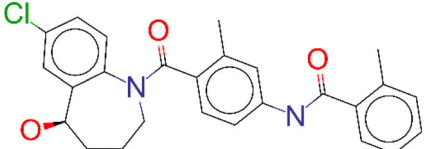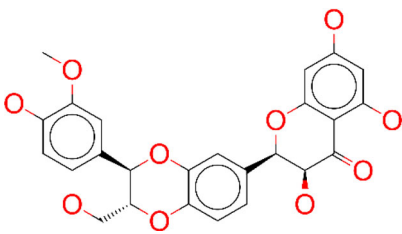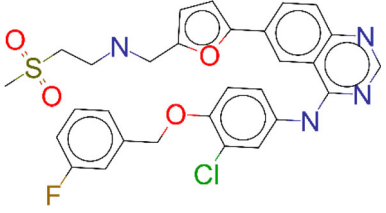
Interestingly, seven of the top 20 drugs identified in docking studies have cytostatic activity and are used in cancer therapy: irinotecan, etoposid, teniposide, doxorubicin, epirubicin, and proscillaridin. It is well known that HIV protease inhibitors exert anticancer activity via two main mechanisms; endoplasmic reticulum stress-unfolded protein response pathway and Akt inhibition (Gantt et al., 2013; Maksimovic-Ivanic et al., 2017). Nelfinavir has also been shown to have in vitro anticancer activity (Gantt et al., 2013). HIV protease inhibitors, including nelfinavir and lopinavir, are

Table 4. List of top 15 drugs having the best binding affinity to RdRp.

ZINC ID and/or Drug Name	2D Structure	Vina Binding Affinity (kcal/mol)	Clinical Trial
ZINC000003932831 / Dutasteride		−9.9	Indicated for the treatment of symptomatic benign prostatic hyperplasia (BPH) in men with an enlarged prostate gland
ZINC000052955754 / Ergotamine		−9.8	For use as therapy to abort or prevent vascular headache
ZINC000004198852 / d-Tubocurarine		−9.5	Used as a diagnosis agent for myasthenia gravis, and also to facilitate the intubation after induction of anesthesia in surgical procedure
ZINC000003784182 / Differin		−9.5	For the topical treatment of comedo, papular and pustular acne (acne vulgaris) of the face, chest or back.
ZINC000011679756 / Eltrombopag		−9.5	Thrombopoietin receptor agonists are pharmaceutical agents that stimulate platelet production in the bone marrow
ZINC000012503187 / Conivaptan		−9.4	For the treatment of euvolemic or hypervolemic hyponatremia in hospitalized patients
ZINC000100016058 / Tipranavir		−9.3	For combination antiretroviral treatment of HIV-1 infected adult patients with evidence of viral replication, who are highly treatment-experienced or have HIV-1 strains resistant to multiple protease inhibitors
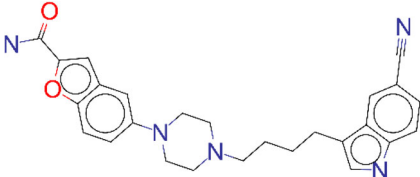
(continued)

Table 4. Continued.

ZINC ID and/or Drug Name	2D Structure	Vina Binding Affinity (kcal/mol)	Clinical Trial
ZINC000003978005 / Dihydroergotamine		−9.3	For the acute treatment of migraine headaches with or without aura and the acute treatment of cluster headache episodes
ZINC000064033452 / Lumacaftor		−9.3	lumacaftor is indicated for the treatment of cystic fibrosis (CF) in patients age 6 years and older who are homozygous for the F508del mutation in the CFTR gene.
ZINC000011681563 / Netupitant		−9.2	for use in combination with palonosetron for the prevention of acute and delayed vomiting and nausea associated with cancer chemotherapy including highly emetogenic chemotherapy
ZINC000253632968 / Simeprevir		−9.2	Indicated for the treatment of adults with chronic hepatitis C virus (HCV) infection:
ZINC000000538658 / Tolvaptan		−9.2	Treatment of symptomatic and resistant to fluid restriction euvolemic or hypervolemic hyponatremia associated with congestive heart failure, and cirrhosis.
ZINC000001757652 / Silibinin		−9.2	Currently being tested as a treatment of severe intoxications with hepatotoxic substances
ZINC000001550477 / Lapatinib		−9.2	Indicated in combination with capecitabine for the treatment of patients with advanced or metastatic breast cancer

Table 4. Continued.

ZINC ID and/or Drug Name	2D Structure	Vina Binding Affinity (kcal/mol)	Clinical Trial
ZINC000001542113 / Vilazodone		−9.2	Vilazodone is approved for treatment of major depressive disorder

peptidomimetics with similar structures and are expected to bind to the nelfinavir docking site in 3CL[pro]. Although several anticancer drugs have displayed in silico interactions with 3CL[pro] ($\leq$ −8.6 kcal/mol), the use of these types of molecules as antiviral therapeutics may not be recommended due to their serious adverse or toxic effects.

3.4. Dockings and MD simulations of tested drugs against RdRp

Docking analyses revealed 850 drugs with docking binding energies lower than −7.5 kcal/mol against the nsp8 binding sites of RdRp (top 100 drugs are listed in Table S2). The top 15 compounds with docking binding energies lower than −9.2 kcal/mol are shown in Table 4, and include ergotamine, dihydroergotamine, bromocriptine, tipranavir, conivaptan, and eltrombopag, which are all well tolerated and widely used.

Notably, ergotamine and its derivatives dihydroergotamine and bromocriptine exhibited high affinities against RdRp, with docking binding energies of −9.8 kcal/mol, −9.3 kcal/mol, and −9.2 kcal/mol, respectively. As explained above, these drugs also exhibited high binding affinities ($<$ −8.6 kcal/mol) against 3CL[pro]. The binding mode of ergotamine showed that it forms hydrogen bonds with backbone oxygen atoms of Thr[324], Phe[326], and Pro[328]. In addition, ergotamine interacts with RdRp via hydrophobic interactions with Val[330] and Val[398] (Figure 7(A)). A complete list of amino acid residues that interact with ergotamine is given in Table 5. We investigated dynamic interactions between ergotamine and RdRp by performing 20 ns MD simulations. Contact analysis from MD showed that Thr[324], Val[330], and Val[398] were critical for drug binding (Figure 7(A)). We also monitored distances between Val[398]/Thr[324] and the geometric center of bound drugs. While ergotamine kept its position in the nsp8 binding site, it got closer to Val[398] as the simulation progressed, with a BFE of −24.65 kcal/mol (Figure 8(A)) (Table 3). Although we did not have a reference molecule to gauge the BFEs of our selected molecules for RdRp, the values calculated for 3CL[pro] indicate that a BFE of approximately −20kcal/mol can be considered as high affinity. Detailed energy decomposition analysis indicated that Val[398] and Thr[324] interacted most strongly with ergotamine (Figure 9). Conservation of these interactions during MD simulations and their contribution to BFE suggests that ergotamine can stably interact with the nsp8 binding site of RdRp. These results indicate that ergotamine and dihydroergotamine are

possible candidates for further in vitro testing and clinical evaluation as an anti-SARS-CoV-2 agents.

Eltrombopag and conivaptan showed high binding affinities of −9.5 kcal/mol and −9.4 kcal/mol, respectively, to the nsp8 binding site of RdRp. While eltrombopag can form hydrogen bonds with Thr[324], Pro[328], and Leu[329], and make hydrophobic interactions with Val[330] and Val[398], conivaptan interacts with only Leu[270] and Val[330] by hydrophobic interactions (Figure 7(B, C)) (Table 5).

Contact analysis indicated that all these polar and hydrophobic interactions were maintained throughout MD simulations for both drugs (Figure 7(B, C)). Measuring distances between the drugs and amino acid residues clearly showed that eltrombopag maintained its original docking position perfectly while conivaptan interacted with only Val[330] (Figure 8(B, C)). BFEs of conivaptan and eltrombopag to RdRp were calculated as −23.83 kcal/mol and −35.33 kcal/mol by MM/GBSA analysis, respectively (Table 3). Analysis of the contributions of critical amino acid residues to BFEs indicated that Val[398]/Thr[324] and Val[329]/Val[330] had the highest impact on the binding of conivaptan and eltrombopag, respectively (Figure 9). All calculations and analysis suggest that eltrombopag can strongly bind to the nsp8 binding site of RdRp and may attenuate its polymerase activity. Interestingly, eltrombopag and conivaptan also showed high binding affinities of −8.2 kcal/mol and −8.7 kcal/mol, respectively, against 3CL[pro].

Eltrombopag is a human thrombopoietin receptor agonist that is used to treat low blood platelet counts in adults with chronic immune (idiopathic) thrombocytopenia (ITP) (Erickson-Miller et al., 2009). The metabolism and disposition of eltrombopag were studied after a single oral administration of a solution dose of [(^{14})C] eltrombopag (75 mg, 100 μCi) and was shown to be a well-tolerated drug (Deng et al., 2011). In vitro analysis revealed that eltrombopag can inhibit severe fever with thrombocytopenia syndrome (SFTS) virus replication. This retrovirus causes SFTS, a newly recognized viral hemorrhagic fever that emerged in rural areas of China and spread to Japan and South Korea (Yu et al., 2011). In a recent in vitro screening study, eltrombopag was shown to have antiviral activity against SARS-CoV-2, with an IC$_{50}$ value of $<$10 μM (Jeon et al., 2020).

Conivaptan inhibits both isotypes of the vasopressin receptor (V$_{1a}$ and V2) and is used for the treatment of euvolemic or hypervolemic hyponatremia (e.g. the syndrome of inappropriate secretion of antidiuretic hormone, or in the setting of hypothyroidism, adrenal insufficiency, pulmonary disorders, etc.) in hospitalized patients. Placebo-controlled, randomized, double-blind, multi-center studies have shown
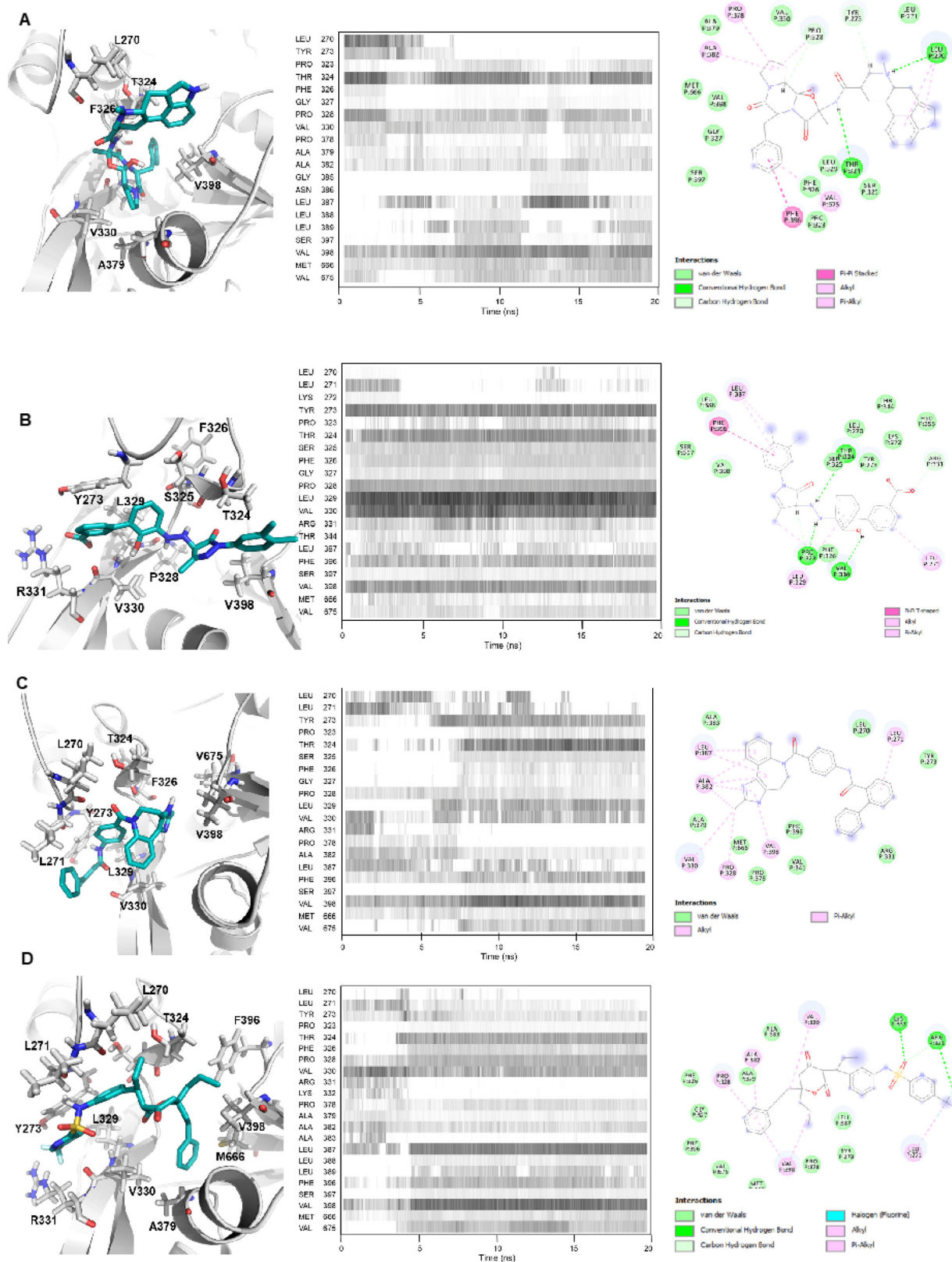
Figure 7. Binding mode of top 4 candidates drugs to RdRp. **A)** ergotamine **B)** eltrombopag **C)** conivaptan and **D)** tipranavir. Docking position of each drug is shown at left panels for each drug. Proteins are shown in ribbon and drugs are shown with stick representations. 20 ns MD simulations were performed and the frequency of interacting amino acid residues are shown in middle panels. Right panel shows the amino acid resides of the SARS-CoV-2 3CL^{pro} that interacts with drugs after molecular simulations. The following coloring scheme is used in figures: carbons are white, nitrogens are blue, oxygens are red, sulphurs are yellow, however, carbons in ligands are shown in cyan.

Table 5. Interacting residues of selected drugs with RdRp.

Drug	Interacting residues
Ergotamine	Leu270, Thr324, Phe326, Val330, Ala379, Val398
Eltrombopag	Tyr273, Val329, Val330, Arg331, Val398
Conivaptan	Leu270, Leu271, Tyr273, Thr324, Phe326, Leu329, Val330, Val398, Val675
Tipranavir	Leu270, Leu271, Tyr273, Thr324, Leu329, Val330, Arg331, Ala379, Phe396, Val398, Met666
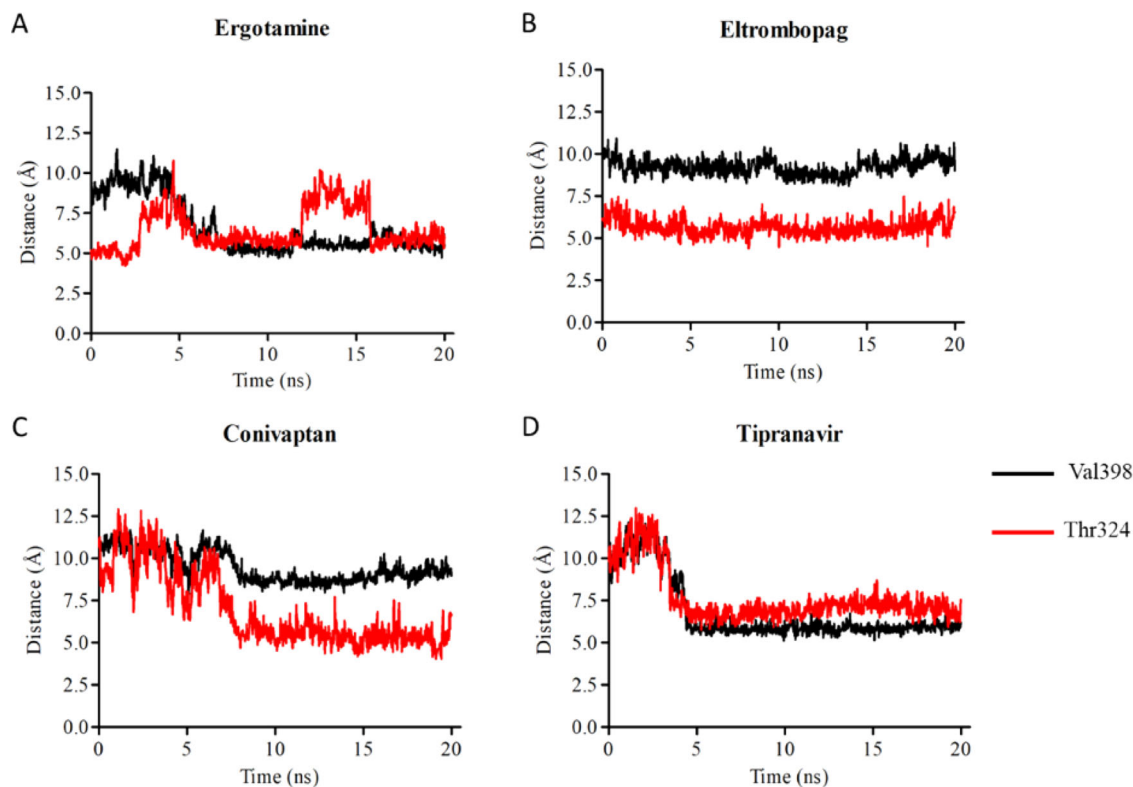
Figure 8. Distance between geometric center of drugs A) ergotamine, B) eltrombopag, C) conivaptan, D) tipranavir and Cα atoms of critical residues (Val[398] and Thr[324]) on RdRp.
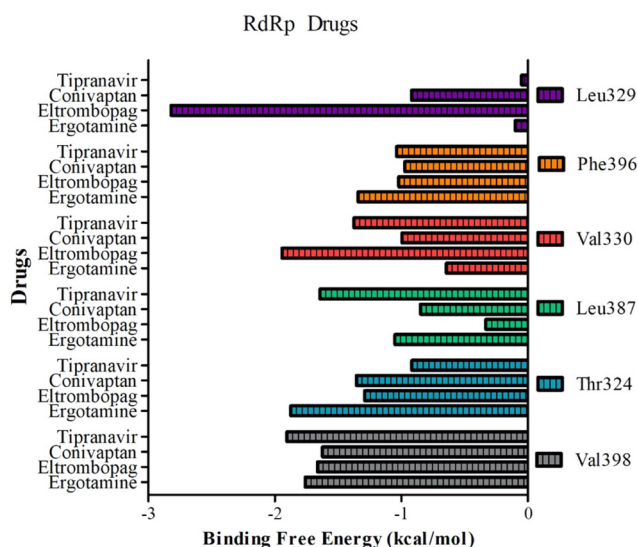
Figure 9. Contribution of each residue to binding free energy in drug-3CL[pro] simulations.

that oral conivaptan is well tolerated in cases with hyponatremia (Annane et al., 2009; Ghali et al., 2006). Conivaptan has antiviral activity against dengue (DENV) and Zika (ZIKV) viruses at high concentrations (IC$_{50}$ >100μM) (Montes-Grajales et al., 2020). Another AVP receptor 2 antagonist, tolvaptan, also has a high binding affinity against RdRp of −9.2 kcal/mol. Like conivaptan, tolvaptan is also used to treat hyponatremia associated with various conditions.

Tipranavir is a sulfonamide-containing dihydropyrone and a nonpeptidic protease inhibitor that targets HIV protease. Interestingly, tipranavir shows high affinities −8.4 kcal/mol and −9.3 kcal/mol against both 3CL[pro] and RdRp, respectively. The binding mode of tipranavir to RdRp suggests that the drug forms a hydrogen bond interaction with backbone oxygen atom of Leu[271] (Figure 7(D)). In addition, fluorine atoms on the trifluoromethylpyridine moiety of tipranavir are within hydrogen bond distance with Arg[331]. Val[330], Phe[396], and Val[398] residues enable hydrophobic interactions between the drug and RdRp (Table 5). While hydrophobic interactions were maintained in MD simulations, interactions with Leu[271] and Arg[331] were not conserved, especially after the first 5 ns of the simulation. Instead, the drug started to interact more frequently with Thr[324] and Leu[389]. Distance analysis between tipranavir and amino acid residues showed that tipranavir gets closer to Val[398] and Thr[324] (Figure 8(D)). BFE of tipranavir to RdRp was calculated as −26.08 kcal/mol by MM/GBSA analysis (Table 3). Decomposition of BFE further confirmed that tipranavir strongly binds to Val[398], Leu[387], Val[330], and Thr[324] (Figure 9).

Taken together, our docking and MD simulation analyses indicate that ergotamine, dihydroergotamine, eltrombopag, conivaptan, and tipranavir bind to the nsp8 binding site of RdRp and could be used to prevent nsp8 binding. These molecules are therefore strong candidates for use in therapies to attenuate the maximum activity of RdRp in SARS-CoV-2.

4. Conclusion

Our in silico analyses revealed several candidates as potential therapeutics against SARS-CoV-2. Tetracycline and its derivatives exhibited high affinity to 3CL^{pro}. These antibiotics are cheap, well tolerated, and the patients may benefit from not only their antibacterial and anti-inflammatory effects, but also their antiviral activity. Dutasteride also exhibited high affinity to 3CL^{pro}. Dutasteride has been shown to down regulate the expression of transmembrane serine protease 2 (TMPRSS2) (Lucas et al., 2008; Mostaghel et al., 2014). It was recently shown that SARS-CoV-2 uses the angiotensin-converting enzyme 2 (ACE2) for entry and TMPRSS2 for S protein priming. SARS-CoV-2 cell entry was blocked by TMPRSS2 protease inhibitor (Hoffmann et al., 2020). COVID-19 patients may benefit from dutasteride due to its effect on TMPRSS2 and ACE2 expression, and its possible antiviral activity. Additionally, ergotamine, dihydroergotamine, bromocriptine, conivaptan, eltrombopag, paliperidone, and tipranavir exhibited strong interaction potential with both 3CL^{pro} and RdRp, and are also among the promising candidates (Table S3). As these drugs are cost-effective and widely used, they can be utilized alone or in combination as an adjuvant with currently used protocols in the treatment of SARS-CoV-2 infection. Additionally, each of the above drugs can be selected for different groups of patients based on their primary effects. For example, dutasteride could be selected for use exclusively in males because of its antiandrogenic effects and eltrombopag could be selected for COVID-19 patients displaying thrombocytopenia. As these drugs have high affinity to both target proteins, these compounds should be less sensitive to genetic variations in SARS-CoV-2 3CL^{pro} and RdRp due to mutations arising during circulation of the virus amongst populations. Because of their target proteins, the above drugs should exert their antiviral effects at the early––mid stage of infection and impair the viral reproductive cycle.

As there are currently no approved therapeutics and vaccines for SARS-CoV-2 infection, in silico repurposing of approved drugs targeting viral proteins still represents a promising approach for discovering new antiviral molecules. Although the results of in silico analysis must be confirmed with in vitro studies and clinical testing, repurposing of commonly used, well-tolerated drugs can help to expedite the drug discovery process during urgent situations.

Disclosure statement

References

Agwuh, K. N., & MacGowan, A. (2006). Pharmacokinetics and pharmacodynamics of the tetracyclines including glycylcyclines. *The Journal of Antimicrobial Chemotherapy*, *58*(2), 256–265. https://doi.org/10.1093/jac/dkl224

Anand, K., Ziebuhr, J., Wadhwani, P., Mesters, J. R., & Hilgenfeld, R. (2003). Coronavirus main proteinase (3CLpro) structure: Basis for design of anti-SARS drugs. *Science (New York, N.Y.)*, *300*(5626), 1763–1767. https://doi.org/10.1126/science.1085658

Andriole, G. L., & Kirby, R. (2003). Safety and tolerability of the dual 5 alpha-reductase inhibitor dutasteride in the treatment of benign prostatic hyperplasia. *European* Urology, *44*(1), 82–88. https://doi.org/10.1016/S0302-2838(03)00198-2

Annane, D., Decaux, G., Smith, N., & Grp, C. S. (2009). Efficacy and safety of oral conivaptan, a vasopressin-receptor antagonist, evaluated in a randomized, controlled trial in patients with euvolemic or hypervolemic hyponatremia. *The* American Journal of the Medical Sciences, *337*(1), 28–36. https://doi.org/10.1097/MAJ.0b013e31817b8148

Armutlu, P., Ozdemir, M. E., Ozdas, S., Kavakli, I. H., & Turkay, M. (2009). Discovery of novel CYP17 inhibitors for the treatment of prostate cancer with structure-based drug design. *Letters in Drug Design & Discovery*, *6*(5), 337–344. https://doi.org/10.2174/1570180810906050337

Boopathi, S., Poma, A. B., & Kolandaivel, P. (2020). Novel 2019 coronavirus structure, mechanism of action, antiviral drug promises and rule out against its treatment. *Journal* of Biomolecular Structure and Dynamics, 1–10. https://doi.org/10.1080/07391102.2020.1758788.

Çakir, B., Dağliyan, O., Dağyildiz, E., Bariş, İ., Kavakli, I. H., Kizilel, S., & Türkay, M. (2012). Structure based discovery of small molecules to regulate the activity of human insulin degrading enzyme. *PLoS One*, *7*(2), e31787. https://doi.org/10.1371/journal.pone.0031787

Chan, J. F., Chik, K. K., Yuan, S., Yip, C. C., Zhu, Z., Tee, K. M., Tsang, J. O., Chan, C. C., Poon, V. K., Lu, G., Zhang, A. J., Lai, K. K., Chan, K. H., Kao, R. Y., & Yuen, K. Y. (2017). Novel antiviral activity and mechanism of bromocriptine as a Zika virus NS2B-NS3 protease inhibitor. *Antiviral Research*, *141*, 29–37. https://doi.org/10.1016/j.antiviral.2017.02.002

Christie, S., Gobel, H., Mateos, V., Allen, C., Vrijens, F., Shivaprakash, M., & Pr, R. E. C. (2003). Crossover comparison of efficacy and preference for rizatriptan 10 mg versus ergotamine/caffeine in migraine. *European Neurology*, *49*(1), 20–29. https://doi.org/10.1159/000067018

Clark, R. V., Hermann, D. J., Cunningham, G. R., Wilson, T. H., Morrill, B. B., & Hobbs, S. (2004). Marked suppression of dihydrotestosterone in men with benign prostatic hyperplasia by dutasteride, a dual 5alpha-reductase inhibitor. *Journal* of Clinical Endocrinology and Metabolism, *89*(5), 2179–2184. https://doi.org/10.1210/jc.2003-030330

Case, D. A., I. Y. B.-S., Brozell, S. R., Cerutti, D. S., Cheatham, T. E., III, Cruzeiro, V. W. D., Darden, T. A., Duke, R. E., Ghoreishi, D., Gilson, M. K., Gohlke, H., Goetz, A. W., Greene, D., Harris, R., Homeyer, N., Izadi, S., Kovalenko, A., Kurtzman, T., Lee, T. S. … Kollman, (2018). *208. AMBER*. University of California.

Das, S., Sarmah, S., Lyndem, S., & Singha Roy, A. (2020). An investigation into the identification of potential inhibitors of SARS-CoV-2 main protease using molecular docking study. *Journal* of Biomolecular Structure and Dynamics, 1–11. https://doi.org/10.1080/07391102.2020.1763201

Davidson, M., Emsley, R., Kramer, M., Ford, L., Gassmann-Mayer, C., Lim, P., Pan, J., & Eerdekens, M. (2006). Efficacy, safety and effect on functioning of oral paliperidone extended-release tablets in the treatment of acute schizophrenia: An International 6-week placebo-controlled study. *Schizophrenia Research*, *81*, 43–43.

De Clercq, E. (2007). The design of drugs for HIV and HCV. *Nature Reviews Drug Discovery*, *6*(12), 1001–1018. https://doi.org/10.1038/nrd2424

DeLano, W. L. (2009). PyMOL molecular viewer: Updates and refinements. In *Abstracts of papers of the American Chemical Society* (Vol. 238). American Chemical Society.

Deng, Y., Madatian, A., Wire, M. B., Bowen, C., Park, J. W., Williams, D., Peng, B., Schubert, E., Gorycki, F., Levy, M., & Gorycki, P. D. (2011). Metabolism and disposition of eltrombopag, an oral, nonpeptide thrombopoietin receptor agonist, in healthy human subjects. *Drug Metabolism and Disposition: The Biological Fate of Chemicals*, *39*(9), 1734–1746. https://doi.org/10.1124/dmd.111.040170

Diener, H. C., Jansen, J. P., Reches, A., Pascual, J., Pitei, D., Steiner, T. J., & St, E. C. C. (2002). Efficacy, tolerability and safety of oral eletriptan and ergotamine plus caffeine (Cafergot (R)) in the acute treatment of migraine: A multicentre, randomised, double-blind, placebo-controlled comparison. *European Neurology*, *47*(2), 99–107. https://doi.org/10.1159/000047960

Doruk, Y. U., Yarparvar, D., Akyel, Y. K., Gul, S., Taskin, A. C., Yilmaz, F., Baris, I., Ozturk, N., Turkay, M., Ozturk, N., Okyar, A., & Kavakli, I. H. (2020). A CLOCK-binding small molecule disrupts the interaction between CLOCK and BMAL1 and enhances circadian rhythm amplitude. *The Journal of Biological Chemistry*, *295*(11), 3518–3531. https://doi.org/10.1074/jbc.RA119.011332

Drosten, C., Gunther, S., Preiser, W., van der Werf, S., Brodt, H. R., Becker, S., Rabenau, H., Panning, M., Kolesnikova, L., Fouchier, R. A., Berger, A., Burguiere, A. M., Cinatl, J., Eickmann, M., Escriou, N., Grywna, K., Kramme, S., Manuguerra, J. C., Muller, S., … Doerr, H. W. (2003). Identification of a novel coronavirus in patients with severe acute respiratory syndrome. *The New England Journal of Medicine*, *348*(20), 1967–1976. https://doi.org/10.1056/NEJMoa030747

Dyall, J., Gross, R., Kindrachuk, J., Johnson, R. F., Olinger, G. G., Hensley, L. E., Frieman, M. B., & Jahrling, P. B. (2017). Middle East respiratory syndrome and severe acute respiratory syndrome: Current therapeutic options and potential targets for novel therapies. *Drugs*, *77*(18), 1935–1966. https://doi.org/10.1007/s40265-017-0830-1

Erickson-Miller, C. L., Delorme, E., Tian, S. S., Hopson, C. B., Landis, A. J., Valoret, E. I., Sellers, T. S., Rosen, J., Miller, S. G., Luengo, J. I., Duffy, K. J., & Jenkins, J. M. (2009). Preclinical activity of eltrombopag (SB-497115), an oral, nonpeptide thrombopoietin receptor agonist. *Stem Cells (Dayton, Ohio)*, *27*(2), 424–430. https://doi.org/10.1634/stemcells.2008-0366

Firth, A. E., & Brierley, I. (2012). Non-canonical translation in RNA viruses. *The Journal of General Virology*, *93*(Pt 7), 1385–1409. https://doi.org/10.1099/vir.0.042499-0

Gantt, S., Casper, C., & Ambinder, R. F. (2013). Insights into the broad cellular effects of nelfinavir and the HIV protease inhibitors supporting their role in cancer treatment and prevention. *Current Opinion in Oncology*, *25*(5), 495–502. https://doi.org/10.1097/CCO.0b013e328363dfee

Ghali, J. K., Koren, M. J., Taylor, J. R., Brooks-Asplund, E., Fan, K., Long, W. A., Smith, N., & Grp, C. S. (2006). Efficacy and safety of oral conivaptan: A V-1A/V-2 vasopressin receptor antagonist, assessed in a randomized, placebo-controlled trial in patients with euvolemic or hypervolemic hyponatremia. *The Journal of Clinical Endocrinology & Metabolism*, *91*(6), 2145–2152. https://doi.org/10.1210/jc.2005-2287

Gorbalenya, A. E., Enjuanes, L., Ziebuhr, J., & Snijder, E. J. (2006). Nidovirales: Evolving the largest RNA virus genome. *Virus Research*, *117*(1), 17–37. https://doi.org/10.1016/j.virusres.2006.01.017

Graham, R. L., Sparks, J. S., Eckerle, L. D., Sims, A. C., & Denison, M. R. (2008). SARS coronavirus replicase proteins in pathogenesis. *Virus Research*, *133*(1), 88–100. https://doi.org/10.1016/j.virusres.2007.02.017

Habibzadeh, P., & Stoneman, E. K. (2020). The novel coronavirus: A bird's eye view. *The International Journal of Occupational and Environmental Medicine*, *11*(2), 65–71. https://doi.org/10.15171/ijoem.2020.1921

He, Y. F., Lian, S. J., & Dong, Y. C. (2020). Clinical characteristics, diagnosis, and treatment of COVID-19: A case report. *World Journal of Clinical Cases*, *8*(11), 2325–2331. https://doi.org/10.12998/wjcc.v8.i11.2325

Hoffmann, M., Kleine-Weber, H., Schroeder, S., Kruger, N., Herrler, T., Erichsen, S., Schiergens, T. S., Herrler, G., Wu, N. H., Nitsche, A., Muller, M. A., Drosten, C., & Pohlmann, S. (2020). SARS-CoV-2 cell entry depends on ACE2 and TMPRSS2 and is blocked by a clinically proven protease inhibitor. *Cell*, *181*(2), 271–280. https://doi.org/10.1016/j.cell.2020.02.052

Huang, J., Rauscher, S., Nawrocki, G., Ran, T., Feig, M., de Groot, B. L., Grubmuller, H., & MacKerell, A. D. Jr., (2017). CHARMM36m: An improved force field for folded and intrinsically disordered proteins. *Nature Methods*, *14*(1), 71–73. https://doi.org/10.1038/nmeth.4067

Humphrey, W., Dalke, A., & Schulten, K. (1996). VMD: Visual molecular dynamics. *Journal of Molecular Graphics*, *14*(1), 33–38. https://doi.org/10.1016/0263-7855(96)00018-5

Irwin, J. J., & Shoichet, B. K. (2005). ZINC-a free database of commercially available compounds for virtual screening. *Journal of Chemical Information and Modeling*, *45*(1), 177–182. https://doi.org/10.1021/ci049714+

Islam, R., Parves, M. R., Paul, A. S., Uddin, N., Rahman, M. S., Mamun, A. A., Hossain, M. N., Ali, M. A., & Halim, M. A. (2020). A molecular modeling approach to identify effective antiviral phytochemicals against the main protease of SARS-CoV-2. *Journal of Biomolecular Structure and Dynamics*, 1–12. https://doi.org/10.1080/07391102.2020.1761883

Janicak, P. G., & Winans, E. A. (2007). Paliperidone ER: A review of the clinical trial data. *Neuropsychiatric Disease and Treatment*, *3*(6), 869–897. https://doi.org/10.2147/ndt.s1365

Jeon, S., Ko, M., Lee, J., Choi, I., Young Byun, S., Park, S., Shum, D., Kim, S. (2020). Identification of antiviral drug candidates against SARS-CoV-2 from FDA-approved drugs. *Antimicrobial Agents and Chemotherapy*, 1–9. https://doi.org/10.1101/2020.03.20.999730.

Jo, S., Kim, T., Iyer, V. G., & Im, W. (2008). CHARMM-GUI: A web-based graphical user interface for CHARMM. *Journal of Computational Chemistry*, *29*(11), 1859–1865. https://doi.org/10.1002/jcc.20945

Kato, F., Ishida, Y., Oishi, S., Fujii, N., Watanabe, S., Vasudevan, S. G., Tajima, S., Takasaki, T., Suzuki, Y., Ichiyama, K., Yamamoto, N., Yoshii, K., Takashima, I., Kobayashi, T., Miura, T., Igarashi, T., & Hishiki, T. (2016). Novel antiviral activity of bromocriptine against dengue virus replication. *Antiviral Research*, *131*, 141–147. https://doi.org/10.1016/j.antiviral.2016.04.014

Khan, R. J., Jha, R. K., Amera, G. M., Jain, M., Singh, E., Pathak, A., Singh, R. P., Muthukumaran, J., & Singh, A. K. (2020). Targeting SARS-CoV-2: A systematic drug repurposing approach to identify promising inhibitors against 3C-like proteinase and 2′-O-ribose methyltransferase. *Journal of Biomolecular Structure and Dynamics*, 1–14. https://doi.org/10.1080/07391102.2020.1753577

Kim, S., Lee, J., Jo, S., Brooks, C. L., 3rd, Lee, H. S., & Im, W. (2017). CHARMM-GUI ligand reader and modeler for CHARMM force field generation of small molecules. *Journal of Computational Chemistry*, *38*(21), 1879–1886. https://doi.org/10.1002/jcc.24829

Kirchdoerfer, R. N., & Ward, A. B. (2019). Structure of the SARS-CoV nsp12 polymerase bound to nsp7 and nsp8 co-factors. *Nature Communications*, *10*(1), 2342. https://doi.org/10.1038/s41467-019-10280-3

Ksiazek, T. G., Erdman, D., Goldsmith, C. S., Zaki, S. R., Peret, T., Emery, S., Tong, S., Urbani, C., Comer, J. A., Lim, W., Rollin, P. E., Dowell, S. F., Ling, A. E., Humphrey, C. D., Shieh, W. J., Guarner, J., Paddock, C. D., Rota, P., Fields, B., … Group, S. W. (2003). A novel coronavirus associated with severe acute respiratory syndrome. *New England Journal of Medicine*, *348*(20), 1953–1966. https://doi.org/10.1056/NEJMoa030781

Kvernmo, T., Hartter, S., & Burger, E. (2006). A review of the receptor-binding and pharmacokinetic properties of dopamine agonists. *Clinical Therapeutics*, *28*(8), 1065–1078. https://doi.org/10.1016/j.clinthera.2006.08.004

Li, H., Zhou, Y., Zhang, M., Wang, H., Zhao, Q., & Liu, J. (2020). Updated approaches against SARS-CoV-2. *Antimicrobial Agents and Chemotherapy*, *64*(6), 1–7. https://doi.org/10.1128/AAC.00483-20

Li, Y. M., Wu, Z. C., Liu, K., Qi, P. F., Xu, J. P., Wei, J. C., Li, B. B., Shao, D. H., Shi, Y. Y., Qiu, Y. F., & Ma, Z. Y. (2017). Doxycycline enhances adsorption and inhibits early-stage replication of porcine reproductive

and respiratory syndrome virus in vitro. *FEMS Microbiology Letters*, *364*, 1–6.

Lim, J., Jeon, S., Shin, H. Y., Kim, M. J., Seong, Y. M., Lee, W. J., Choe, K. W., Kang, Y. M., Lee, B., & Park, S. J. (2020). Case of the index patient who caused tertiary transmission of COVID-19 infection in Korea: The application of Lopinavir/Ritonavir for the treatment of COVID-19 infected pneumonia monitored by quantitative RT-PCR. *Journal of Korean Medical Science*, *35*(6), e79. https://doi.org/10.3346/jkms.2020.35.e89

Lo, H. S., Hui, K. P. Y., Lai, H.-M., Khan, K. S., Kaur, S., Li, Z., Chan, A. K. N., Cheung, H. H.-Y., Ng, K. C., Ho, J. C. W., Chen, Y. W., Ma, B., Cheung, P. M.-H., Shin, D., Wang, K., Wu, K.-P., Dikic, I., Liang, P.-H., Zuo, Z., … Ng, W.-L. (2020). Simeprevir suppresses SARS-CoV-2 replication and synergizes with remdesivir. *bioRxiv*, 1–20. https://doi.org/10.1101/2020.05.26.116020

Lucas, J., True, L., Hawley, S., Matsumura, M., Morrissey, C., Vessella, R., & Nelson, P. (2008). The androgen-regulated type II serine protease TMPRSS2 is differentially expressed and mislocalized in prostate adenocarcinoma. *The Journal of Pathology*, *215*(2), 118–125. https://doi.org/10.1002/path.2330

Madeira, F., Park, Y. M., Lee, J., Buso, N., Gur, T., Madhusoodanan, N., Basutkar, P., Tivey, A. R. N., Potter, S. C., Finn, R. D., & Lopez, R. (2019). The EMBL-EBI search and sequence analysis tools APIs in 2019. *Nucleic Acids Research*, *47*(W1), W636–W641. https://doi.org/10.1093/nar/gkz268

Maksimovic-Ivanic, D., Fagone, P., McCubrey, J., Bendtzen, K., Mijatovic, S., & Nicoletti, F. (2017). HIV-protease inhibitors for the treatment of cancer: Repositioning HIV protease inhibitors while developing more potent NO-hybridized derivatives? *International Journal of Cancer*, *140*(8), 1713–1726. https://doi.org/10.1002/ijc.30529

Marberger, M. (2006). Drug Insight: 5alpha-reductase inhibitors for the treatment of benign prostatic hyperplasia. *Nature Clinical Practice. Urology*, *3*(9), 495–503. https://doi.org/10.1038/ncpuro0577

Marder, S. R., Kramer, M., Ford, L., Eerdekens, E., Lim, P., Eerdekens, M., & Lowy, A. (2007). Efficacy and safety of paliperidone extended-release tablets: Results of a 6-week, randomized, placebo-controlled study. *Biological Psychiatry*, *62*(12), 1363–1370. https://doi.org/10.1016/j.biopsych.2007.01.017

Montes-Grajales, D., Puerta-Guardo, H., Espinosa, D. A., Harris, E., Caicedo-Torres, W., Olivero-Verbel, J., & Martinez-Romero, E. (2020). In silico drug repurposing for the identification of potential candidate molecules against arboviruses infection. *Antiviral Research*, *173*, 104668 https://doi.org/10.1016/j.antiviral.2019.104668

Mortier, E., Pouchot, J., Vinceneux, P., & Lalande, M. (2001). Ergotism related to interaction between nelfinavir and ergotamine. *The American Journal of Medicine*, *110*(7), 594–594. https://doi.org/10.1016/S0002-9343(01)00655-6

Mostaghel, E. A., Nelson, P. S., Lange, P., Lin, D. W., Taplin, M. E., Balk, S., Ellis, W., Kantoff, P., Marck, B., Tamae, D., Matsumoto, A. M., True, L. D., Vessella, R., Penning, T., Merrill, R. H., Gulati, R., & Montgomery, B. (2014). Targeted androgen pathway suppression in localized prostate cancer: A pilot study. *Journal of Clinical Oncology*, *32*(3), 229–237. https://doi.org/10.1200/JCO.2012.48.6431

Musarrat, F., Chouljenko, V., Dahal, A., Nabi, R., Chouljenkpo, T., Jois, S. D., & Kousoulas, K. (2020). The anti-HIV drug nelfinavir mesylate (Viracept) is a potent inhibitor of cell fusion caused by the SARSCoV-2 spike (S) glycoprotein warranting further evaluation as an antiviral against COVID-19 infections. *Journal of Medical Virology*, 1–9. https://doi.org/10.1002/jmv.25985

Owen, C. D., Lukacik, P., Strain-Damerell, C. M., Douangamath, A., Powell, A. J., Fearon, D., Brandao-Neto, J., Crawshaw, A. D., Aragao, D., Williams, M., Flaig, R., Hall, D. R., McAuley, K. E., Mazzorana, M., Stuart, D. I., von Delft, F., & Walsh, M. A. (2020). COVID-19 main protease with unliganded active site (2019-nCoV, coronavirus disease 2019, SARS-CoV-2). *CSB Protein Data Bank (PDB) ID, 6Y84*, 3–7. https://doi.org/10.2210/pdb6Y84.

Phillips, J. C., Braun, R., Wang, W., Gumbart, J., Tajkhorshid, E., Villa, E., Chipot, C., Skeel, R. D., Kale, L., & Schulten, K. (2005). Scalable molecular dynamics with NAMD. *Journal of Computational Chemistry*, *26*(16), 1781–1802. https://doi.org/10.1002/jcc.20289

Prajapat, M., Sarma, P., Shekhar, N., Avti, P., Sinha, S., Kaur, H., Kumar, S., Bhattacharyya, A., Kumar, H., Bansal, S., & Medhi, B. (2020). Drug targets for corona virus: A systematic review. *Indian Journal of Pharmacology*, *52*(1), 56–65. https://doi.org/10.4103/ijp.IJP_115_20

Roehrborn, C. G., Boyle, P., Nickel, J. C., Hoefner, K., Andriole, G., Aria, A., & Investigators, A. S. (2002). Efficacy and safety of a dual inhibitor of 5-alpha-reductase types 1 and 2 (dutasteride) in men with benign prostatic hyperplasia. *Urology*, *60*(3), 434–441. https://doi.org/10.1016/S0090-4295(02)01905-2

Rosenthal, E., Sala, F., Chichmanian, R. M., Batt, M., & Cassuto, J. P. (1999). Ergotism related to concurrent administration of ergotamine tartrate and indinavir. *Jama*, *281*(11), 987 https://doi.org/10.1001/jama.281.11.987

Rothan, H. A., Mohamed, Z., Paydar, M., Abd Rahman, N., & Yusof, R. (2014). Inhibitory effect of doxycycline against dengue virus replication in vitro. *Archives of Virology*, *159*(4), 711–718. https://doi.org/10.1007/s00705-013-1880-7

Sarma, P., Shekhar, N., Prajapat, M., Avti, P., Kaur, H., Kumar, S., Singh, S., Kumar, H., Prakash, A., Dhibar, D. P., & Medhi, B. (2020). In-silico homology assisted identification of inhibitor of RNA binding against 2019-nCoV N-protein (N terminal domain). *Journal of Biomolecular Structure and Dynamics*, 1–9.

Scandella, E., Eriksson, K. K., Hertzig, T., Drosten, C., Chen, L., Gui, C., Luo, X., Shen, J., Shen, X., Siddell, S. G., Ludewig, B., Jiang, H., Gunther, S., & Thiel, V. (2006). Identification and evaluation of coronavirus replicase inhibitors using a replicon cell line. *Advances in Experimental Medicine and Biology*, *581*, 609–613. https://doi.org/10.1007/978-0-387-33012-9_111

Silberstein, S. D. (1997). The pharmacology of ergotamine and dihydroergotamine. *Headache*, *37* (Suppl 1), S15–S25.

Sk, M. F., Roy, R., Jonniya, N. A., Poddar, S., & Kar, P. (2020). Elucidating biophysical basis of binding of inhibitors to SARS-CoV-2 main protease by using molecular dynamics simulations and free energy calculations. *Journal of Biomolecular Structure and Dynamics*, 1–13. https://doi.org/10.1080/07391102.2020.1768149

Smilack, J. D. (1999). The tetracyclines. *Mayo Clinic Proceedings*, *74*(7), 727–729. https://doi.org/10.4065/74.7.727

St John, S. E., Tomar, S., Stauffer, S. R., & Mesecar, A. D. (2015). Targeting zoonotic viruses: Structure-based inhibition of the 3C-like protease from bat coronavirus HKU4-The likely reservoir host to the human coronavirus that causes Middle East Respiratory Syndrome (MERS). *Bioorganic & Medicinal Chemistry*, *23*(17), 6036–6048. https://doi.org/10.1016/j.bmc.2015.06.039

Su, S., Wong, G., Shi, W., Liu, J., Lai, A. C. K., Zhou, J., Liu, W., Bi, Y., & Gao, G. F. (2016). Epidemiology, genetic recombination, and pathogenesis of coronaviruses. *Trends in Microbiology*, *24*(6), 490–502. https://doi.org/10.1016/j.tim.2016.03.003

Tardu, M., Rahim, F., Kavakli, I. H., & Turkay, M. (2016). Milp-hyperbox classification for structure-based drug design in the discovery of small molecule inhibitors of Sirtuin6. *RAIRO - Operations Research*, *50*(2), 387–400. https://doi.org/10.1051/ro/2015042

Thiel, V., Ivanov, K. A., Putics, Á., Hertzig, T., Schelle, B., Bayer, S., Weißbrich, B., Snijder, E. J., Rabenau, H., Doerr, H. W., Gorbalenya, A. E., & Ziebuhr, J. (2003). Mechanisms and enzymes involved in SARS coronavirus genome expression. *The Journal of General Virology*, *84*(9), 2305–2315. https://doi.org/10.1099/vir.0.19424-0

Thomson, A. (2005). Dutasteride: An evidence-based review of its clinical impact in the treatment of benign prostatic hyperplasia. *Core Evidence*, *1*(2), 143–156.

Tomar, S., Johnston, M. L., St John, S. E., Osswald, H. L., Nyalapatla, P. R., Paul, L. N., Ghosh, A. K., Denison, M. R., & Mesecar, A. D. (2015). Ligand-induced dimerization of Middle East Respiratory Syndrome (MERS) Coronavirus nsp5 Protease (3CLpro): Implications for nsp5 regulation and the development of antivirals. *The Journal of Biological Chemistry*, *290*(32), 19403–19422. https://doi.org/10.1074/jbc.M115.651463

Trott, O., & Olson, A. J. (2010). AutoDock Vina: Improving the speed and accuracy of docking with a new scoring function, efficient optimization, and multithreading. *Journal of Computational Chemistry*, *31*(2), 455–461. https://doi.org/10.1002/jcc.21334

Via, M. A., Chandra, H., Araki, T., Potenza, M. V., & Skamagas, M. (2010). Bromocriptine approved as the first medication to target dopamine activity to improve glycemic control in patients with type 2 diabetes. *Diabetes, Metabolic Syndrome and Obesity: Targets and Therapy*, *3*, 43–48. https://doi.org/10.2147/DMSO.S9575

WHO. (2020). *WHO Director-General's remarks at the media briefing on 2019-nCoV*. Retrieved February 11, 2020, from https://www.who.int/dg/speeches/detail/who-director-general-s-remarks-at-the-media-briefing-on-2019-ncov-on-11-february-2020.

Wu, C., Liu, Y., Yang, Y., Zhang, P., Zhong, W., Wang, Y., Wang, Q., Xu, Y., Li, M., Li, X., Zheng, M., Chen, L., & Li, H. (2020). Analysis of therapeutic targets for SARS-CoV-2 and discovery of potential drugsby computational methods. *Acta Pharmaceutica Sinica B*, *10*(5), 766–788. https://doi.org/10.1016/j.apsb.2020.02.008

Wu, F., Zhao, S., Yu, B., Chen, Y. M., Wang, W., Song, Z. G., Hu, Y., Tao, Z. W., Tian, J. H., Pei, Y. Y., Yuan, M. L., Zhang, Y. L., Dai, F. H., Liu, Y., Wang, Q. M., Zheng, J. J., Xu, L., Holmes, E. C., & Zhang, Y. Z. (2020). A new coronavirus associated with human respiratory disease in China. *Nature*, *579*(7798), 265–269. https://doi.org/10.1038/s41586-020-2202-3

Wu, Z. C., Wang, X., Wei, J. C., Li, B. B., Shao, D. H., Li, Y. M., Liu, K., Shi, Y. Y., Zhou, B., Qiu, Y. F., & Ma, Z. Y. (2015). Antiviral activity of doxycycline against vesicular stomatitis virus in vitro. *FEMS Microbiology Letters*, *362*, 1–7.

Xu, X., Liu, Y., Weiss, S., Arnold, E., Sarafianos, S. G., & Ding, J. (2003). Molecular model of SARS coronavirus polymerase: Implications for biochemical functions and drug design. *Nucleic Acids Research*, *31*(24), 7117–7130. https://doi.org/10.1093/nar/gkg916

Yamamoto, N., Yang, R. G., Yoshinaka, Y., Amari, S., Nakano, T., Cinatl, J., Rabenau, H., Doerr, H. W., Hunsmann, G., Otaka, A., Tamamura, H., Fujii, N., & Yamamoto, N. (2004). HIV protease inhibitor nelfinavir inhibits replication of SARS-associated coronavirus. *Biochemical and Biophysical Research Communications*, *318*(3), 719–725. https://doi.org/10.1016/j.bbrc.2004.04.083

Yu, X. J., Liang, M. F., Zhang, S. Y., Liu, Y., Li, J. D., Sun, Y. L., Zhang, L., Zhang, Q. F., Popov, V. L., Li, C., Qu, J., Li, Q., Zhang, Y. P., Hai, R., Wu, W., Wang, Q., Zhan, F. X., Wang, X. J., Kan, B., … Li, D. X. (2011). Fever with thrombocytopenia associated with a novel bunyavirus in China. *The New England Journal of Medicine*, *364*(16), 1523–1532. https://doi.org/10.1056/NEJMoa1010095

Yuan, S., Chan, J. F., den-Haan, H., Chik, K. K., Zhang, A. J., Chan, C. C., Poon, V. K., Yip, C. C., Mak, W. W., Zhu, Z., Zou, Z., Tee, K. M., Cai, J. P., Chan, K. H., de la Pena, J., Perez-Sanchez, H., Ceron-Carrasco, J. P., & Yuen, K. Y. (2017). Structure-based discovery of clinically approved drugs as Zika virus NS2B-NS3 protease inhibitors that potently inhibit Zika virus infection in vitro and in vivo. *Antiviral Research*, *145*, 33–43. https://doi.org/10.1016/j.antiviral.2017.07.007

Zaki, A. M., van Boheemen, S., Bestebroer, T. M., Osterhaus, A. D. M. E., & Fouchier, R. A. M. (2012). Isolation of a novel coronavirus from a man with pneumonia in Saudi Arabia. *The New England Journal of Medicine*, *367*(19), 1814–1820. https://doi.org/10.1056/NEJMoa1211721

Zhou, P., Yang, X. L., Wang, X. G., Hu, B., Zhang, L., Zhang, W., Si, H. R., Zhu, Y., Li, B., Huang, C. L., Chen, H. D., Chen, J., Luo, Y., Guo, H., Jiang, R. D., Liu, M. Q., Chen, Y., Shen, X. R., Wang, X., … Shi, Z. L. (2020). A pneumonia outbreak associated with a new coronavirus of probable bat origin. *Nature*, *579*(7798), 270–273. https://doi.org/10.1038/s41586-020-2012-7

Ziebuhr, J. (2004). Molecular biology of severe acute respiratory syndrome coronavirus. *Current Opinion in Microbiology*, *7*(4), 412–419. https://doi.org/10.1016/j.mib.2004.06.007

Ziebuhr, J. (2005). The coronavirus replicase. *Current Topics in Microbiology and Immunology*, *287*, 57–94. https://doi.org/10.1007/3-540-26765-4_3